Inorganic Chemistry

Article

pubs.acs.org/IC

Ligand Contributions to the Electronic Structures of the Oxidized Cobalt(II) salen Complexes

Amélie Kochem,[†] Hussein Kanso,[†] Benoit Baptiste,[†] Himanshu Arora,[†] Christian Philouze,[†] Olivier Jarjayes,[†] Hervé Vezin,[‡] Dominique Luneau,[§] Maylis Orio,[‡] and Fabrice Thomas*[,†]

[†]Equipe de Chimie Inorganique Redox Biomimétique, Département de Chimie Moléculaire, Université Joseph Fourier, 38041 Grenoble Cedex 9, France

[‡]Laboratoire de Spectrochimie Infrarouge et Raman, Université des Sciences et Technologies de Lille, UMR CNRS 8516, 59655 Villeneuve d'Ascq Cedex, France

[§]Laboratoire des Multimatériaux et Interfaces, Groupe de Crystallographie et Ingénierie Moléculaire, Université Claude Bernard Lyon 1, UMR CNRS 5615, Bâtiment Berthollet-Domaine Scientifique de la Doua, 69622 Villeurbanne Cedex, France

Supporting Information

ABSTRACT: Square planar cobalt(II) complexes of salen ligands *N*,*N*′-bis(3-*tert*-butyl-5*R*-salicylidene)-1,2-cyclohexanediamine), where R = OMe (**1**) and *tert*-butyl (**2**), were prepared. **1** and **2** were electrochemically reversibly oxidized into cations $[\mathbf{1}\text{-}H_2O]^+$ and $[\mathbf{2}\text{-}H_2O]^+$ in CH_2Cl_2. The chemically generated $[\mathbf{1}\text{-}H_2O](SbF_6)\cdot 0.68\ H_2O\cdot 0.82CH_2Cl_2$ and $[\mathbf{2}\text{-}H_2O](SbF_6)\cdot 0.3H_2O\cdot 0.85CH_2Cl_2$ were characterized by X-ray diffraction and NIR spectroscopy. Both complexes are paramagnetic species containing a square pyramidal cobalt ion coordinated at the apical position by an exogenous water molecule. They exhibit remarkable NIR bands at 1220 (7370 M^{-1} cm^{-1}) and 1060 nm (5560 M^{-1} cm^{-1}), respectively, assigned to a CT transition. DFT calculations and magnetic measurements confirm the paramagnetic (S = 1) ground spin state of the cations. They show that more than 70% of the total spin density in $[\mathbf{1}\text{-}H_2O]^+$ and $[\mathbf{2}\text{-}H_2O]^+$ is localized on the metal, the remaining spin density being distributed over the aromatic rings (30% phenoxyl character). In the presence of *N*-methylimidazole **1** and **2** are irreversibly oxidized by air into the genuine octahedral cobalt(III) bis(phenolate) complexes $[\mathbf{1}\text{-}im_2]^+$ and $[\mathbf{2}\text{-}im_2]^+$, the former being structurally characterized. Neither $[\mathbf{1}\text{-}im_2]^+$ nor $[\mathbf{2}\text{-}im_2]^+$ exhibits a NIR feature in its electronic spectrum. **1** and **2** were electrochemically two-electron oxidized into $[\mathbf{1}]^{2+}$ and $[\mathbf{2}]^{2+}$. The cations were identified as Co(III)−phenoxyl species by their characteristic absorption band at ca. 400 nm in the UV−vis spectrum. Coordination of the phenoxyl radical to the cobalt(III) metal ion is evidenced by the EPR signal centered at g = 2.00.

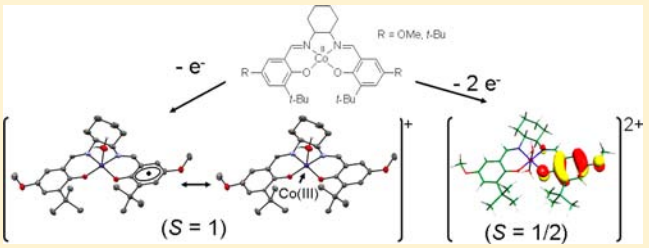

INTRODUCTION

The coordination chemistry of transition-metal ions with pro-radical phenolate ligands has attracted considerable research interest since the elucidation of the electronic structure of the active site of galactose oxidase (GO).[1] GO uses an active site constituted of a single copper ion to catalyze the two-electron oxidation of several alcohols into aldehydes. Initially, it was proposed that the copper ion was at its +III oxidation state and acting as a two-electron oxidant toward substrates.[2] Later, exhaustive spectroscopic characterization ruled out this hypothesis, and it is now established that the active site is rather a tyrosyl radical coordinated to a copper(II) ion.[3] Both the metal and the radical centers, which usually support one-electron redox chemistry when they are alone, work here in synergy to promote a very efficient two-electron oxidative chemistry. This fascinating bioinorganic chemistry was a source of inspiration for chemists who subsequently synthesized many phenoxyl radical complexes, especially from tetradentate Schiff base ligands.[4] During the past decade a number of salen-radical complexes involving first-row transition metals (mainly copper,[5,6] nickel,[6,7] zinc,[8] and iron[9]) were developed, but surprisingly, very few examples of cobalt radical salen complex were reported.[10]

Recently, we focused our attention on the oxidative chemistry of cobalt−tetrahydrosalen complexes and established that one-electron oxidation of the phenolate−cobalt(II) entity was metal centered, affording the phenolate−cobalt(III) complexes.[11] We herein extend our investigation to cobalt complexes involving tetradentate Schiff bases. This study was motivated by the fact that this class of cobalt complexes is of widespread importance in catalysis,[12] for instance, in the ring opening of epoxides[13] and oxidation of alcohols.[14] In both reactions the active species is the monocationic form of the complex or its neutral form if an additional anionic exogenous ligand (chloride, acetate) is axially ligated. The catalyst for ring

Received: April 13, 2012
Published: September 26, 2012

   dx.doi.org/10.1021/ic300763t | *Inorg. Chem.* 2012, 51, 10557−10571

opening of epoxides is prepared in two steps. The ligand is first reacted with $Co(OAc)_2$, affording a Co(II)−bis(phenolate) complex. In the second step, the resulting species is one-electron oxidized either with air (in the presence of acetic acid) or a chemical reagent (one-electron oxidant such as cationic ferrocenium) to give the active catalyst.[13] In principle, one-electron oxidation of a phenolate complex (Co^{II}−L) could afford either the metal−ligand radical (Co^{II}−$L^{\bullet}$) or the (Co^{III}−L) form according to eq 1. Surprisingly, only the cobalt(III)−bis(phenolate) salen, and not the cobalt(II)−phenoxyl form, is considered to be the one-electron oxidation product (and thus the active catalyst).

$$M^{n+}-L \underset{+e^-}{\overset{-e^-}{\rightleftharpoons}} M^{(n+1)+}-L \text{ or } M^{N+}-\dot{L} \quad (1)$$

Determining the electronic structure of one-electron-oxidized Co(II)−bis(phenolate) salen complexes is of prime importance for unravelling catalytic pathways and enhance turnover rates. Recently, Benisvy et al. investigated the oxidative chemistry of tetracoordinated cobalt(II) complexes involving two bidentate imidazole−phenolate chelators, i.e., ligand systems that exhibit strong analogies to the salicylidene family (Figure 1a).[15] They nicely showed that the one-electron-oxidized species are comprised of one phenoxyl radical and one phenolate moiety bound to a Co(II) metal ion and not a cobalt(III)−bis(phenolate) entity. On the other hand, it has been reported that reaction of cobalt(II) salts with 2 equiv of sterically hindered aminobenzophenols affords cobalt(II) complexes involving two coordinated *o*-iminobenzosemiquinonate radical ligands (Figure 1b).[16,17] Interestingly, such complexes could be also isolated in a square pyramidal cobalt(III) form with two coordinated *o*-iminobenzosemiquinonate ligands when an axial anionic ligand is present (Figure 1c).[18,19] Benzenedithiolate and *o*-phenylenediamine ligands were also found to undergo one-electron oxidation, affording the dithiosemiquinonate and *o*-diiminobenzosemiquinonate radicals, respectively, when coordinated to cobalt(II).[18,20] In the corresponding anionic square planar complexes Wieghardt et al. demonstrated that strong metal−ligand orbital mixing occurs, providing both metal and ligand character to the singly occupied molecular orbital (SOMO).[20] It should be emphasized that the radical character of the SOMO in the above cobalt complexes was evidenced by combined theoretical, structural, and spectroscopic methods. From these studies it appears that a good spectroscopic marker for cobalt(II) systems involving a combination of a quinone-like and a coordinated semiquinone-like radical is the presence of a ligand-to-ligand charge transfer transition in the near-infrared (NIR) region of the absorption spectra.[18−20]

The visible spectrum of the one-electron-oxidized form of the Co(II)−bis(phenolate) complex of the Jacobsen ligand (**2** in Scheme 1) was reported recently.[21] Although the complex was believed to be a Co(III)−bis(phenolate) species it displays absorptions in the whole visible region, as well as an intense absorption band at >900 nm,[21] which resembles the signature of Co(II) radical complexes. In this article we investigate the relevance of phenoxyl radicals in the one- and two-electron-oxidized forms of two cobalt(II) salen complexes **1** and **2** (Scheme 1). We show that the electronic structure of the one-electron-oxidized cobalt(II) salen derivatives $[\mathbf{1}\text{-}\mathbf{H_2O}]^+$ and $[\mathbf{2}\text{-}\mathbf{H_2O}]^+$ is solvent dependent and that radical forms are relevant. In the presence of strong exogenous donors (such as *N*-methylimidazole) a metal-centered oxidation process is observed, affording the genuine octahedral Co(III)−bis(phenolate) complexes $[\mathbf{1}\text{-}\mathbf{im_2}]^+$ and $[\mathbf{2}\text{-}\mathbf{im_2}]^+$. When one-electron oxidation is performed in neat CH_2Cl_2 the paramagnetic complexes $[\mathbf{1}\text{-}\mathbf{H_2O}]^+$ and $[\mathbf{2}\text{-}\mathbf{H_2O}]^+$ are obtained. A strong metal−ligand orbital mixing occurs in the complexes, which confers both metal and ligand character to the SOMO. The two-electron-oxidized species $[\mathbf{1}]^{2+}$ and $[\mathbf{2}]^{2+}$ are Co(III)−phenoxyl radical complexes irrespective of the medium and phenolate substituent.

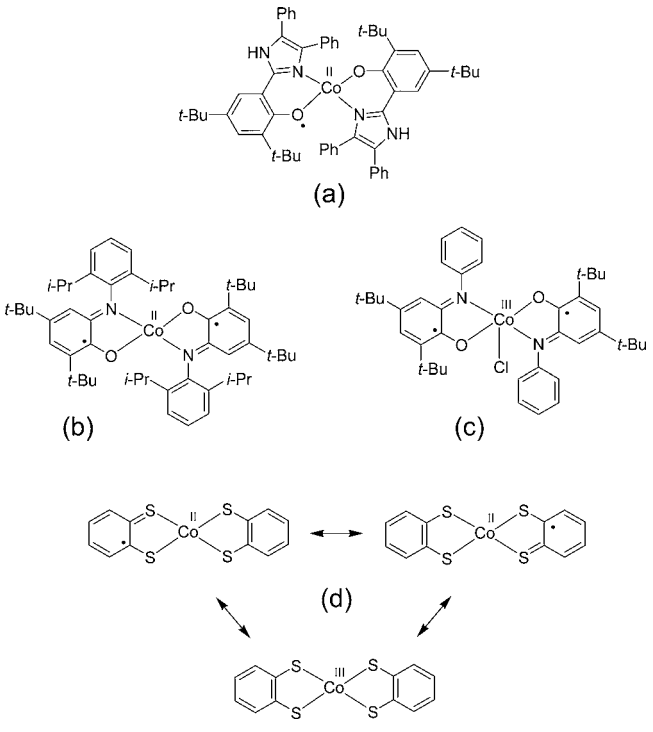

Figure 1. Examples of radical cobalt complexes involving iminobenzosemiquinonate and dithiosemiquinonate ligands.

Scheme 1. Structure of the Initial Neutral Cobalt Complexes Investigated in This Study

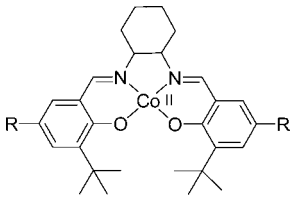

EXPERIMENTAL SECTION

Materials and Methods. X-band and Q-band EPR spectra were recorded on a BRUKER EMX Plus spectrometer controlled with the Xenon software and equipped with a Bruker teslameter. A Bruker nitrogen flow cryostat connected to a high-sensitivity resonant cavity was used for 100 K measurements. An Oxford Instrument Helium flow cryostat connected to a dual-mode resonant cavity was used to run experiments at 10 K. Spectra were simulated using the SIMFONIA software (BRUKER). NMR spectra were recorded on a BRUKER AM 300 (^{1}H at 300 MHz, ^{13}C at 75 MHz). Chemical shifts are given relative to tetramethylsilane (TMS). Mass spectra were recorded on a Thermofinnigen (EI/DCI) apparatus. Microanalyses were performed

dx.doi.org/10.1021/ic300763t | Inorg. Chem. 2012, 51, 10557−10571

by the Service Central d'Analyze du CNRS (Lyon, France). UV−vis−NIR spectra at 298 K were recorded on a Perkin-Elmer Lambda 1050 spectrophotometer equipped with a temperature controller unit set at 298 K. The quartz cell path length was 1 cm. UV−vis spectra at 240 K were recorded on a Cary 50 spectrophotometer equipped with a Hellma low-temperature immersion probe (1 cm path length quartz cell). Temperature was controlled with a Lauda RK8 KS cryostat. Cyclic voltammetry curves were recorded on a CHI 620 potentiostat in a standard three-electrode cell under argon atmosphere. An $AgNO_3$/Ag (0.01 M) reference electrode was used. All potentials given in the text are referenced against the Fc^+/Fc couple. A vitrous carbon disk electrode (5 mm diameter) polished with 1 μm diamond paste was used as working electrode. Electrolysis was performed on a PAR 273 potentiostat, under argon atmosphere at −40 °C, using a carbon felt working electrode.

Crystal Structure Analysis. Collected reflections were corrected for Lorentz and polarization effects but not for absorption in the case of **1** and $[\mathbf{1\text{-}H_2O}](\mathbf{SbF_6})\cdot\mathbf{0.68H_2O}\cdot\mathbf{0.82CH_2Cl_2}$. For the other structures SADABS-2004/1 was used for absorption correction. Structures were solved by direct methods and refined using the TEXSAN[22] and OLEX2 software.[23] All non-hydrogen atoms were refined with anisotropic thermal parameters. Hydrogen atoms were generated in idealized positions, riding on the carrier atoms, with isotropic thermal parameters except the hydroxyl ones, which were localized on the Fourier map and fixed.

Magnetic Measurements. Magnetic susceptibility versus temperature (2−300 K) was measured on a powder sample of $[\mathbf{1\text{-}H_2O}](\mathbf{SbF_6})\cdot\mathbf{0.68H_2O}\cdot\mathbf{0.82CH_2Cl_2}$ using a SQUID magnetometer from Quantum Design model MPMS-XL in an applied magnetic field of 0.1 T. Magnetization versus magnetic field (0−0.5 T) was measured at 2 K. All data were corrected for the contribution of the sample holder, and the diamagnetism of the samples was estimated from Pascal's constants.[24]

Computational Details. All theoretical calculations were performed with the ORCA program package.[25] Full geometry optimizations[26] were carried out for all complexes using the GGA functional BP86[27−29] in combination with the TZV/P[30] basis set for all atoms and by taking advantage of the resolution of the identity (RI) approximation in the Split-RI-J variant[31] with the appropriate Coulomb fitting sets.[32] Increased integration grids (Grid4 in ORCA convention) and tight SCF convergence criteria were used. Solvent effects were accounted for according to the experimental conditions. For that purpose, we used the CH_2Cl_2 (ε = 9.08) solvent within the framework of the conductor-like screening (COSMO) dielectric continuum approach.[33] Relative energies were obtained from single-point calculations using the B3LYP[34,35] functional together with the TZV/P[30] basis set. They were computed from the gas-phase-optimized structures as a sum of electronic energy, thermal corrections to free energy, and free energy of solvation. Optical properties were also obtained from single-point calculations using the hybrid functional B3LYP[34,35] and the TZV/P[30] basis set. Electronic transition energies and dipole moments for all models were calculated using time-dependent DFT (TD-DFT)[36−38] within the Tamm−Dancoff approximation.[39,40] To increase computational efficiency, the RI approximation[41] was used in calculating the Coulomb term and at least 30 excited states were calculated in each case. Both *g* tensors and hyperfine coupling constants were obtained from single-point calculations employing the hybrid functional B3LYP.[34,35] The triply polarized core property basis set CP(PPP)[42] was applied for the metal, while the EPR-II[43] basis set was used for all remaining atoms. Special care was also taken to ensure accurate results by increasing the size of the integration grid to 7 (ORCA convention) for the metal center.[42]

Synthesis. ***1***. To a suspended solution of the enantiopure *R,R* ligand (0.05 g, 0.11 mmol) in methanol was added dropwise and under an inert atmosphere a methanolic solution of $Co(OAc)_2\cdot 4H_2O$ (0.024 g, 0.11 mmol) and triethylamine (31 μL, 0.22 mmol). The resulting reaction mixture was stirred and heated at reflux for 2 h. A brown precipitate appeared and was filtered, washed with cold methanol, and dried under vacuum. Yield: 0.040 g (65%). Anal. Calcd for $C_{30}H_{40}CoN_2O_4$ (551.58): C, 65.32; H, 7.31; N, 5.08; Co, 10.68. Found: C, 71.06; H, 7.02; N, 4.98. ESI-MS *m/z*: 551.2 $[M + H]^+$.

[1-H₂O](SbF₆). To a solution of **1** (0.04 g, 0.0725 mmol) in CH_2Cl_2 (10 mL) was added $AgSbF_6$ (0.027 g, 0.0797 mmol) under an inert atmosphere. This solution was stirred for 30 min at room temperature until a silver mirror was formed and then filtered through Celite. The resultant solution of $[\mathbf{1\text{-}H_2O}](\mathbf{SbF_6})$ was concentrated. Vapor diffusion of pentane into this solution afforded dark brown single crystals of formula $[\mathbf{1\text{-}H_2O}](\mathbf{SbF_6})\cdot\mathbf{0.68H_2O}\cdot\mathbf{0.82CH_2Cl_2}$ that were collected by filtration. Yield: 0.043 g (75%). Anal. Calcd for $C_{30}H_{42}CoF_6N_2O_5Sb\cdot H_2O\cdot CH_2Cl_2$ (908.3): C, 40.99; H, 5.10; N, 3.08; Co, 6.49. Found: C, 45.60; H, 4.98; N, 3.64. ESI-MS *m/z*: 551.2 $[M - SbF_6]^+$ and 235.8 $[SbF_6]^-$.

$[\mathbf{2\text{-}H_2O}](\mathbf{SbF_6})$ was prepared in an identical manner to $[\mathbf{1\text{-}H_2O}](\mathbf{SbF_6})$ with the enantiopure *R,R* ligand. Dark brown single crystals of formula $[\mathbf{1\text{-}H_2O}](\mathbf{SbF_6})\cdot\mathbf{0.3H_2O}\cdot\mathbf{0.85CH_2Cl_2}$ were collected by filtration. Yield: 0.048 g (67%). Anal. Calcd for $C_{36}H_{54}CoF_6N_2O_3Sb\cdot CH_2Cl_2$ (942.4): C, 47.15; H, 5.99; N, 2.97; Co, 6.25. Found: C, 46.60; H, 6.02; N, 2.86. ESI-MS *m/z*: 621.3 $[M - SbF_6]^+$ and 235.8 $[SbF_6]^-$.

[1-im₂](ClO₄). To complex **1** (0.016 g, 0.029 mmol) in a methanol/CH_2Cl_2 solution (5/5 mL) was added 3 equiv of 2-methylimidazole (0.087 mmol). The solution was stirred at room temperature for 2 h and turned dark red. $NaClO_4\cdot H_2O$ (0.0245 g, 0.174 mmol) in methanol (2 mL) was then added, and stirring at room temperature was continued for 1 day. Slow evaporation of the solvent gave dark red crystals after 1 day that were collected by filtration, washed with cold methanol, and dried under vacuum. Yield: 0.020 g (85%). Anal. Calcd for $C_{38}H_{52}ClCoN_8O_6$ (811.26): C, 56.26; H, 6.46; N, 4.37; Co, 7.26. Found: C, 56.46; H, 6.24; N, 4.42. ESI-MS *m/z*: 715.4 $[M - ClO_4]^+$. ^1H NMR (CD_3OD, 300 MHz) (ppm): 8.09 (s, 2H, CH═N), 7.22−7.21 (m, 2H, Me-Im ring), 7.035 (d, ^4J = 3.3 Hz, 2H, Ar−H), 6.92−6.90 (t, ^3J = 1.5 Hz, 2H, Me-Im ring), 6.835 (d, ^4J = 3.3 Hz, 2H, Ar−H), 6.51−6.50 (t, ^3J = 1.5 Hz, 2H, Me-Im ring), 3.80 (s, 6H, CH_3−Im), 3.58 (s, 6H, CH_3O), 3.26 (d, 2H, chiral H), 2.98 (d, 2H, CH_2), 2.06 (d, 2H, CH_2) 1.85 (m, 2H, CH_2), m (1.52, 2H, CH_2), 1.40 (s, 18H, tBu).

RESULTS AND DISCUSSION

Synthesis of the Ligands and Complexes. Ligands (under their chiral *R,R* form) were synthesized according to published methods (R = OMe)[6] or purchased from Sigma Aldrich (R = tBu). Low-spin cobalt(II) complexes **1** and **2** were readily obtained by metalation of the corresponding ligand with $Co(OAc)_2\cdot 4H_2O$ under anaerobic conditions in methanol. Single crystals of **1** were obtained by slow evaporation of a concentrated methanolic solution. Aerobic oxidation of a methanolic:CH_2Cl_2 solution of **1** in the presence of 3 mol equiv of N-methylimidazole followed by addition of $NaClO_4$ affords the diamagnetic complex $[\mathbf{1\text{-}im_2}](\mathbf{ClO_4})$. Single crystals were grown by slow evaporation of a concentrated methanolic solution of $[\mathbf{1\text{-}im_2}](\mathbf{ClO_4})$. We prepared $[\mathbf{2\text{-}im_2}](\mathbf{ClO_4})$ according to a published procedure.[44] When the one-electron oxidation of **1** or **2** was realized by addition of 1 mol equiv of $AgSbF_6$ in the noncoordinating solvent CH_2Cl_2 the paramagnetic species $[\mathbf{1\text{-}H_2O}](\mathbf{SbF_6})$ and $[\mathbf{2\text{-}H_2O}](\mathbf{SbF_6})$ were obtained. Single crystals of $[\mathbf{1\text{-}H_2O}](\mathbf{SbF_6})\cdot\mathbf{0.68H_2O}\cdot\mathbf{0.82CH_2Cl_2}$ and $[\mathbf{2\text{-}H_2O}](\mathbf{SbF_6})\cdot\mathbf{0.3H_2O}\cdot\mathbf{0.85CH_2Cl_2}$ were grown by slow diffusion of pentane into concentrated CH_2Cl_2 solutions of these complexes. The $[\mathbf{1\text{-}im_2}]^+$ complex could alternatively be prepared by addition of *N*-methylimidazole to a CH_2Cl_2 solution of $[\mathbf{1\text{-}H_2O}](\mathbf{SbF_6})\cdot\mathbf{0.68H_2O}\cdot\mathbf{0.82CH_2Cl_2}$. In this case $[\mathbf{1\text{-}im_2}]^+$ is obtained either as $\mathbf{SbF_6^-}$ ($[\mathbf{1\text{-}im_2}](\mathbf{SbF_6})\cdot\mathbf{1.13im}$) or $\mathbf{Cl^-}$ salt ($[\mathbf{1\text{-}im_2}](\mathbf{Cl})\cdot\mathbf{4H_2O}$); the chloride ion likely arises from reaction with the solvent).

dx.doi.org/10.1021/ic300763t | *Inorg. Chem.* 2012, 51, 10557−10571

Table 1. Crystallographic Data for 1, $[1\text{-}H_2O](SbF_6)\cdot 0.68H_2O\cdot 0.82CH_2Cl_2$, and $[1\text{-}im_2](ClO_4)$

formula	1	$[1\text{-}H_2O](SbF_6)\cdot 0.68H_2O\cdot 0.82CH_2Cl_2$	$[1\text{-}im_2](ClO_4)$
M	551.59	882.92	815.24
cryst syst	triclinic	monoclinic	orthorhombic
space group	$P1$	$P12_11$	$P2_12_12_1$
a/Å	8.949[1]	10.338[1]	9.206[2]
b/Å	11.835[2]	14.007[2]	19.005(5)
c/Å	13.649[2]	13.438[2]	22.744(7)
α/deg	77.16[1]	90	90
β/deg	72.86[1]	104.88[1]	90
γ/deg	85.70[2]	90	90
V/Å^3	1346.8(4)	1880.5(3)	3979.5[2]
Z	2	2	4
T/K	200	200	200
D_c/g·cm^{-3}	1.360	1.559	1.361
μ (cm^{-1})	6.76	13.45	5.56
monochromator	graphite	graphite	graphite
wavelength	Mo Kα (0.71073)	Mo Kα (0.71073)	Mo Kα (0.71073)
independent reflns (R_{int})	13 821 (0.0711)	10 678 (0.0678)	6989 (0.0451)
obs reflns	11 150 ($I > 2\sigma(I)$)	9200 ($I > 2\sigma(I)$)	5852 ($I > 2\sigma(I)$)
R	0.0462	0.0470	0.0438
R_w	0.1011	0.1092	0.1018

Geometric and Electronic Structure of the Neutral Complexes. The crystal cell of **1** (Table 1) contains two distinct molecules (A and B). The solid state structure of one, arbitrary chosen, is shown in Figure 2, while that of **2** has been previously reported.[45] **1** displays a cobalt(II) ion coordinated by two oxygens O1, O2 and two nitrogens N1, N2, with a small angle between the O1−Co−N1 and O2−Co−N2 planes of 0.9° and 9.4° (molecules A and B, respectively) and O1−Co−O2, O1−Co−N1, O2−Co−N2, and N1−Co−N2 angles that differ only slightly from 90° (87.1[2]°, 93.2[2]°, 94.0[2]°, and 86.5[2]°, respectively, in molecule A, 87.4[2]°, 93.4[2]°, 86.4[2]°, and 92.8[2]°, respectively, in molecule B). The geometry around the metal ion is thus essentially square planar. The Co−O1, Co−O2, Co−N1, and Co−N2 bond lengths are 1.835[4], 1.847[4], 1.861[5], and 1.864[5] Å, respectively, in molecule A (1.848[4], 1.855[4], 1.851[5], and 1.852[5] Å, respectively, in molecule B), consistent with a low-spin configuration for the cobalt(II) ion, which has been further confirmed by EPR spectroscopy (see below). Not surprisingly, both aromatic rings exhibit methoxyphenolate character, with C1−O1 and C13−O2 bond lengths of 1.297(7) and 1.311(7) Å and C4−O3 and C16−O4 (opposite C−methoxy bonds) of 1.380(6) and 1.382(6) Å, respectively, in molecule A (corresponding bond distances in molecule B are 1.327(7), 1.309(7), 1.378(7), and 1.390(7) Å).

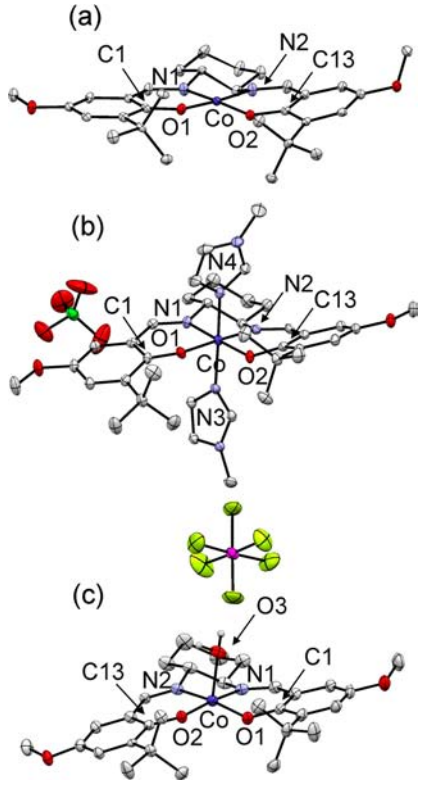

Figure 2. X-ray crystal structures of (a) **1**, (b) $[1\text{-}im_2](ClO_4)$, and (c) $[1\text{-}H_2O](SbF_6)$ shown with 30% thermal ellipsoids. H atoms are omitted except those of the coordinated water molecule in $[1\text{-}H_2O]^+$.

The geometry around the metal ion in the previously reported structure of **2**[45] is very close to that observed for **1**, with almost identical Co−O1 and Co−O2 bond distances (Table 2). It is noteworthy that the Co−N1 and Co−N2 bond lengths reported for **2** are longer by 0.04 and 0.02 Å, respectively, when compared to **1** and other cobalt(II) bis(phenolate) salen complexes.[46] However, given the poor quality of this crystal structure, within error we assume that it is the same length as in **1**.

Table 2. Comparison of Experimental and Calculated Coordination Sphere Bond Lengths (Angstroms) for 1 and 2

bond	1 (exp), molecule A	1 (exp), molecule B	1 (calcd)	2 (exp)[45]	2 (calcd)
Co−O1	1.835(4)	1.848(4)	1.850	1.84(1)	1.851
Co−O2	1.847(4)	1.855(4)	1.850	1.84(1)	1.853
Co−N1	1.861(5)	1.851(5)	1.858	1.89(1)	1.860
Co−N2	1.864(5)	1.852(5)	1.858	1.87(1)	1.861

DFT calculations using DFT methods were performed for the two systems **1** and **2** by considering an $S = 1/2$ ground spin state (Figures S1 and S2, Supporting Information). Bond

dx.doi.org/10.1021/ic300763t | Inorg. Chem. 2012, 51, 10557−10571

distances calculated by geometry optimization match those of the X-ray structures by 0.01 Å (Table 2) in the case of **1**. As expected, the calculated Co−O and Co−N bond distances do not differ significantly on going from **1** and **2**.

The 10 K X-band EPR spectrum of **1** in CH_2Cl_2 is depicted in Supporting Information Figure S1. It displays an anisotropic ($S = 1/2$) signal with hyperfine splitting into eight lines in the low-field component. This pattern arises from the interaction of the electron spin with the cobalt nucleus ($I_{Co} = 7/2$). The spectrum could be simulated with the set of parameters $g_x = 2.92$, $g_y = 1.91$, $g_z = 2.03$ ($g_{iso} = 2.29$), and $A_{x(Co)} = 210$ MHz (the other hyperfine coupling constants could not be determined from simulation). It is noteworthy that the values determined for **1** are close to the ones reported for **2** ($g_x = 3.21$, $g_y = 1.89$, $g_z = 1.98$, ($g_{iso} = 2.36$),[10] thus confirming that the overall geometry of the complexes in solution is very similar. These parameters point to a main $d_{z^2}^1$ orbital ground state. EPR data are thus consistent with a square planar geometry for a d^7 metal ion and indicate that the cobalt(II) complex retains its solid state structure in CH_2Cl_2 solution. DFT calculations on the geometry-optimized complexes **1** and **2** confirm the metal-based character of the SOMO for both **1** (56% d_{z2}, 40% d_{yz}) and **2** (53% d_{z2}, 43% d_{yz}) as shown in Supporting Information Figures S10 and S11.

Visible spectra of **1** and **2** are characterized by intense transitions at 423 (17 330 M^{-1} cm^{-1}) and 419 nm (12 990 M^{-1} cm^{-1}), respectively, with weaker d−d bands above 500 nm (Figure 3, Table 3). On the basis of its high intensity the highest energy absorption is assigned to a charge transfer (CT) transition. The exact nature of the orbitals involved in the CT transition was investigated by TD-DFT calculations. In both **1** and **2** the principal calculated electronic excitation that contributes to the CT band is a βHOMO−3 → βLUMO+1 transition ($\lambda_{calcd} = 470$ nm, $f = 0.146$ for **1** and $\lambda_{calcd} = 467$ nm, $f = 0.197$ for **2**). In both cases, the donor orbital is a pure metal orbital (d_{xz}) while the acceptor one is a delocalized π orbital involving the β-iminoalkoxy moiety with a small d_{x2-y2} contribution (Figure 4, Table 4). Although the computed

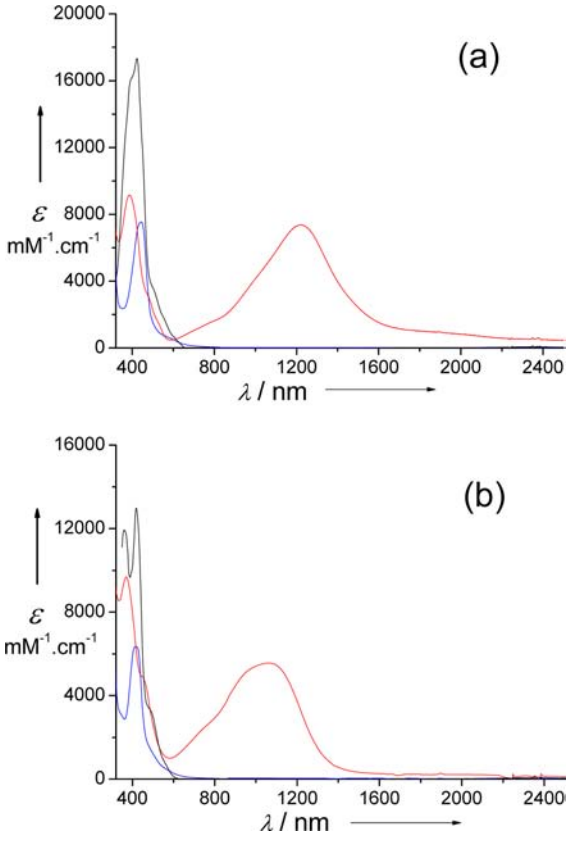

Figure 3. Vis−NIR spectra of solutions of the neutral and one-electron oxidized complexes in 0.05 mM CH_2Cl_2 solutions: (a) **1** (black), [**1-im$_2$**]$^+$ (blue), and [**1-H$_2$O**]$^+$ (red); (b) **2** (black), [**2-im$_2$**]$^+$ (blue), and [**2-H$_2$O**]$^+$ (red). $T = 298$ K.

Table 3. Electronic Spectral Data of the Complexes[a]

complex	λ_{max}, nm (ε, M^{-1} cm^{-1})
1	390 (15850), 423 (17330), 509sh (3370), 557sh (1710)
[**1-im$_2$**]$^+$	444 (7550), 584br (600)
[**1-H$_2$O**]$^+$	386 (9150), 1217br (7370)
[**1**]$^{2+}$	408 (8120)[b]
2	359 (11940), 419 (12990), 499sh (3040)
[**2-im$_2$**]$^+$	416 (6340)
[**2-H$_2$O**]$^+$	372 (9690), 452sh (4880), 1060br (5560)
[**2**]$^{2+}$	402 (7720), 800br (1420)[b]

[a] In CH_2Cl_2 solution, $T = 298$ K. Abbreviations used: sh, shoulder; br, broad. [b] In CH_2Cl_2 + 0.01 M TBAP solution, $T = 240$ K.

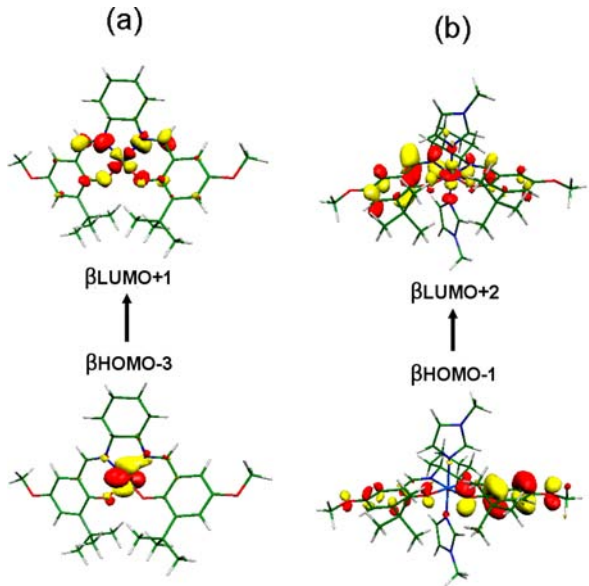

Figure 4. TD-DFT assignment of the lowest energy transition in (a) **1** and (b) [**1-im$_2$**]$^+$.

Table 4. Lowest Energy Calculated Electronic Excitations of the Complexes[a]

complex	transition (MO number)	λ, nm (f)
1	βHOMO−3→ βLUMO+1	470 (0.146)
[**1-im$_2$**]$^+$	βHOMO−1→ βLUMO+2	496 (0.126)
[**1-H$_2$O**]$^+$[b]	βHOMO−2→ βLUMO	1013 (0.110)
[**1-H$_2$O**]$^+$[c]	βHOMO → βLUMO+2	1183 (0.210)
2	βHOMO−3→ βLUMO+1	467 (0.197)
[**2-im$_2$**]$^+$	βHOMO−1→ βLUMO+2	433 (0.082)
[**2-H$_2$O**]$^+$[b]	βHOMO−2→ βLUMO+1	952 (0.158)
[**2-H$_2$O**]$^+$[c]	βHOMO→ βLUMO+2	1154 (0.103)

[a] In CH_2Cl_2. [b] Triplet state. [c] Quintet state.

dx.doi.org/10.1021/ic300763t | Inorg. Chem. 2012, 51, 10557−10571

energy for the transition is slightly higher than the experimental one, calculations correctly predict the absence of a significant shift on going from **1** to **2**.

Electrochemistry. The electrochemical behavior of the square planar cobalt(II) complexes **1** and **2** has been studied by cyclic voltammetry (CV) in the noncoordinating solvent CH_2Cl_2 (+0.1 M TBAP). All potentials are referenced versus the Fc^+/Fc redox couple. Both **1** and **2** are electroactive in the potential range from −1.0 to +1.0 V. The CV curves of **1** and **2** display three reversible one-electron redox waves in the anodic region of potentials (Figure 5, Table 5). Oxidation potentials are summarized in Table 5.

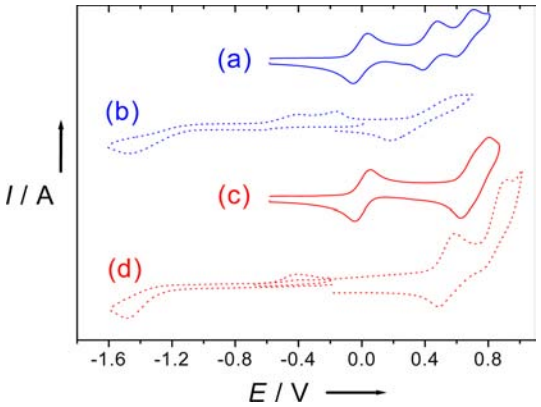

Figure 5. CV curves of 0.5 mM solutions of **1** and **2** in CH_2Cl_2 (+0.1 M TBAP): (a) **1** in CH_2Cl_2; (b) $[\mathbf{1\text{-}im_2}]^+$ in CH_2Cl_2 + 10 equiv of *N*-methylimidazole; (c) **2** in CH_2Cl_2; (d) $[\mathbf{2\text{-}im_2}]^+$ in CH_2Cl_2 + 10 equiv of *N*-methylimidazole. Potentials are given vs the Fc^+/Fc reference. Scan rate: 0.1 V/s; T = 298 K.

Table 5. Electrochemical Properties of 1 and 2 in CH_2Cl_2 Solutions[a]

complex	$E_p^{a,1}$	$E_p^{c,1}$	$E_{1/2}^{1}$	$E_p^{a,2}$	$E_p^{c,2}$	$E_{1/2}^{2}$	$E_{1/2}^{3}$
1	0.04	−0.04	0.00	0.49	0.39	0.44	0.62
$[\mathbf{1\text{-}im_2}]^+$	−0.23	−1.61	−0.92	0.70	0.14	0.42	
$[\mathbf{1\text{-}im_2}]^{+b}$	−0.40	−1.48	−0.94	0.65	0.19	0.42	
2	0.06	−0.04	0.01	0.65	0.75	0.70[c]	0.74[c]
$[\mathbf{2\text{-}im_2}]^+$		−1.43		0.59	0.49	0.55	
$[\mathbf{2\text{-}im_2}]^{+b}$	−0.40	−1.48	−0.94	0.59	0.49	0.55	

[a]In the presence of 0.1 M TBAP. Potential values given in V vs the Fc^+/Fc reference electrode, T = 298 K. [b]In the presence of 10 equiv of imidazole. [c]Measured by DPV given the close proximity of $E_{1/2}$.

The redox processes are observed at $E_{1/2}^{1}$ = 0.00 V, $E_{1/2}^{2}$ = 0.44 V, and $E_{1/2}^{3}$ = 0.62 V for **1** and $E_{1/2}^{1}$ = 0.01 V, $E_{1/2}^{2}$ = 0.70 V, and $E_{1/2}^{3}$ = 0.74 V vs Fc^+/Fc for **2**. The position of the first redox wave does not depend on the nature of the phenolate substituent. At first glance this oxidation process may be attributed to a metal-centered process; nevertheless, a non-negligible contribution of the ligand to the SOMO was evidenced spectroscopically in the one-electron-oxidized species (see below). The redox couple is therefore not purely metal based. The second and third oxidation waves are strongly substituent dependent and correspond to successive formation of the Co^{3+}−phenoxyl and Co^{3+}−bis(phenoxyl) species according to eq 2. Interestingly, the electrochemical communication between the noninnocent phenolate rings is much smaller in **2** than in **1**, as reflected by the smaller $\Delta E = E_{1/2}^{3} - E_{1/2}^{2}$ in **2**.

$$Co^{2+}\text{–}L \overset{E_{1/2}^{1}}{\rightleftharpoons} Co^{2+}\text{–}L^{\cdot} \text{ or } Co^{3+}\text{–}L \overset{E_{1/2}^{2}}{\rightleftharpoons} Co^{3+}\text{–}L^{\cdot} \overset{E_{1/2}^{3}}{\rightleftharpoons} Co^{3+}\text{–}L^{\cdot\cdot} \quad (2)$$

The CV of the genuine octahedral cobalt(III)−bis-(phenolate) complexes $[\mathbf{1\text{-}im_2}]^+$ and $[\mathbf{2\text{-}im_2}]^+$ prepared by air oxidation of **1** and **2**, respectively, in the presence of *N*-methylimidazole (see below for full characterization) are shown in Figure 5. $[\mathbf{1\text{-}im_2}]^+$ and $[\mathbf{2\text{-}im_2}]^+$ exhibit an irreversible reduction wave at $E_p^{c,1}$ = −1.61 V and $E_p^{c,1}$ = −1.43 V, respectively. The reduction peak is associated with an oxidation one at $E_p^{a,1}$ = −0.23 V for $[\mathbf{1\text{-}im_2}]^+$ (peak separation ΔE_p^{1} of 1.38 V), while no oxidation signal could be detected for $[\mathbf{2\text{-}im_2}]^+$. The large peak separation ΔE_p^{1} indicates that a significant molecular rearrangement (ligand exchange, see below) occurs during the redox process. After addition of 10 equiv of *N*-methylimidazole to the medium the ΔE_p^{1} value of $[\mathbf{1\text{-}im_2}]^+$ decreases to 1.08 V ($E_p^{c,1}$ = −1.48 V; $E_p^{a,1}$ = −0.40 V) while the $E_p^{a,1}$ peak of $[\mathbf{2\text{-}im_2}]^+$ (which was absent in neat CH_2Cl_2) could be detected at $E_p^{a,1}$ = −0.40 V ($E_p^{c,1}$ = −1.48 V, giving a ΔE_p^{1} value of 1.08 V). The large peak separation ΔE_p^{1} as well as the half-wave potentials $E_{1/2}^{1}$ (−0.94 V, roughly estimated as a midpoint potential between $E_p^{c,1}$ and $E_p^{a,1}$, the redox couple being chemically irreversible) are thus identical for $[\mathbf{1\text{-}im_2}]^+$ and $[\mathbf{2\text{-}im_2}]^+$ in a medium containing CH_2Cl_2 + 10 equiv of *N*-methylimidazole. This indicates that the redox process is metal centered (Co(III)/Co(II) redox couple).[47,48] The decrease in ΔE_p^{1} resulting from addition of *N*-methylimidazole to the medium is clear evidence that a molecular rearrangement occurs upon reduction of the octahedral cobalt(III) complex.[48] It is attributed to release of *N*-methylimidazole in the medium upon reduction, which affords the square planar cobalt(II) complexes **1** and **2**. It is noteworthy that axial ligation by the *N*-methylimidazole base greatly stabilizes the cobalt(III) complex, as reflected by the lower $E_p^{c,1}$ of $[\mathbf{1\text{-}im_2}]^+$ and $[\mathbf{2\text{-}im_2}]^+$ when compared to **1** and **2**.[47] Examination of the second oxidation process reveals a dramatic difference between $[\mathbf{1\text{-}im_2}]^+$ and $[\mathbf{2\text{-}im_2}]^+$. The peak separation ΔE_p^{2} is found to be abnormally high (ΔE_p^{2} > 0.5 V) and dependent on the concentration of *N*-methylimidazole in the case of $[\mathbf{1\text{-}im_2}]^+$, whereas it is 0.10 V and not dependent on the *N*-methylimidazole concentration in the case of $[\mathbf{2\text{-}im_2}]^+$. We interpret this behavior by either a release of the *N*-methylimidazole ligand of $[\mathbf{1\text{-}im_2}]^+$ upon oxidation or slow electrode kinetics. In order to obtain insight on the origin of the phenomenon we synthesized a derivative of $[\mathbf{1\text{-}im_2}]^+$ that bears an ethylene bridge instead of the cyclohexylidene one but maintains the 2-*tert*-butyl-4-methoxyphenolate moieties.[48] For this complex we observed an anodic signal at $E_{1/2}^{2}$ = 0.33 V, i.e., a value close to the one observed for **1**, with a much smaller ΔE_p^{2} value of 0.08 V. This supports the fact that the large ΔE_p^{2} of $[\mathbf{1\text{-}im_2}]^+$ arises from slow electrode kinetics, although we cannot definitely rule out changes in coordination upon oxidation. Interestingly, the half-wave potentials $E_{1/2}^{2}$ (calculated as the midpoint between the $E_p^{a,2}$ and the $E_p^{c,2}$ values) are found to range between 0.42 and 0.55 V for all compounds. $E_{1/2}^{2}$ values are almost identical in $[\mathbf{1\text{-}H_2O}]^+$ and $[\mathbf{1\text{-}im_2}]^+$ (0.44 and 0.42 V, respectively), while they differ by 0.15 V when $[\mathbf{2\text{-}H_2O}]^+$ is compared to $[\mathbf{2\text{-}im_2}]^+$ (0.70 and 0.55 V, respectively). $E_{1/2}^{1}$ values are observed in a much larger potential window (from −0.94 to 0.01 V for all compounds), the lower ones being observed for the *N*-methylimidazole complexes. The large stabilization of the monocation by

dx.doi.org/10.1021/ic300763t | *Inorg. Chem.* 2012, 51, 10557−10571

imidazole is consistent with a metal-based redox process in the first oxidation, and its lack of influence upon the other oxidations implies that they are ligand centered.

Characterization of the One-Electron-Oxidized Complexes in the Presence of *N*-Methylimidazole. In the presence of *N*-methylimidazole oxidation of the neutral species **1** into the corresponding monocation was realized simply by aerobic incubation due to the low $E_{1/2}^1$ value under these conditions (see electrochemistry discussion).[49] Addition of $NaClO_4$ to the resulting solution initiates crystallization of the diamagnetic $[\mathbf{1\text{-}im_2}](\mathbf{ClO_4})$ complex.[50] Its structure is depicted in Figure 2, and the coordination bond lengths are summarized in Table 6. The cobalt ion in $[\mathbf{1\text{-}im_2}]^+$ resides in an octahedral geometry with two *N*-methylimidazole ligands coordinated at both apical positions. This geometry is very similar to the one reported for $[\mathbf{2\text{-}im_2}]^+$.[44] The two *N*-methylimidazole ligands are coordinated at the Co−N3 and Co−N4 bond distances 1.965(3) and 1.955(3) Å, respectively. The bond lengths in the equatorial plane Co−O1, Co−O2, Co−N1, and Co−N2 are 1.896[2], 1.881[2], 1.900(3), and 1.893(3) Å, respectively, with a very small angle between the O1−Co−N1 and the O2−Co−N2 planes of 2.8° (a value of 4.4° was reported for $[\mathbf{2\text{-}im_2}]^+$). Of interest is the significant lengthening (ca. 0.05 Å) of the equatorial coordination bonds when $[\mathbf{1\text{-}im_2}]^+$ is compared to **1**, which evidence a change in the oxidation state of the metal ion upon oxidation.[44] Accordingly, examination of the C1−O1 and C13−O2 bond lengths in $[\mathbf{1\text{-}im_2}]^+$ reveal that these bond distances are essentially unaffected by oxidation (1.318 and 1.314 Å in $[\mathbf{1\text{-}im_2}]^+$, respectively, vs 1.318 and 1.315 Å in **1**). The overall structure and bond distances in the cations $[\mathbf{1\text{-}im_2}](\mathbf{SbF_6})\cdot\mathbf{1.13im}$ and $[\mathbf{1\text{-}im_2}](\mathbf{Cl})\cdot\mathbf{4H_2O}$ are very similar to the ones obtained for $[\mathbf{1\text{-}im_2}](\mathbf{ClO_4})$; thus, they will not be commented upon in detail (Supporting Information Figure S2).

Table 6. Comparison of Experimental and Calculated Coordination Sphere Bond Lengths [Angstroms] for the One-Electron-Oxidized $[\mathbf{1\text{-}im_2}]^+$ and $[\mathbf{2\text{-}im_2}]^+$ [a]

bond	$[\mathbf{1\text{-}im_2}]^+$ (exp)	$[\mathbf{1\text{-}im_2}]^+$ (calcd)	$[\mathbf{2\text{-}im_2}]^+$ (exp)[44]	$[\mathbf{2\text{-}im_2}]^+$ (calcd)
Co−O1	1.896(2)	1.914	1.881(3)	1.923
Co−O2	1.881(2)	1.905	1.883(3)	1.905
Co−N1	1.900(3)	1.917	1.882(4)	1.917
Co−N2	1.893(3)	1.909	1.869(4)	1.904
Co−N3	1.965(3)	1.974	1.938(5)	1.973
Co−N4	1.955(3)	1.962	1.930(4)	1.961

[a] Experimental distances measured in the $[\mathbf{1\text{-}im_2}](\mathbf{ClO_4})$ and $[\mathbf{2\text{-}im_2}](\mathbf{ClO_4})$ salts

The $[\mathbf{1\text{-}im_2}]^+$ complex was found to be diamagnetic in solution, as reflected by the sharp ^1H resonances distributed over a small spectral window in $CDCl_3$. X-ray diffraction and NMR data are thus consistent with the fact that $[\mathbf{1\text{-}im_2}]^+$ is a genuine low-spin octahedral cobalt(III)−bis(phenolate) complex.[44]

DFT calculations were performed on both $[\mathbf{1\text{-}im_2}]^+$ and $[\mathbf{2\text{-}im_2}]^+$ by considering a singlet ground spin state (low-spin cobalt(III) metal ion) for the complexes. As shown in Table 6, the experimental lengthening of the equatorial Co−O and Co−N bonds is well predicted by geometry optimization in both systems. The computed bond distances match those of the X-ray structures within 0.02 Å for $[\mathbf{1\text{-}im_2}]^+$ and 0.035 Å for $[\mathbf{2\text{-}im_2}]^+$, the axial bonds being not surprisingly the least accurately calculated. The metal ion geometry is also perfectly predicted, with a calculated deviation of the coordinating atoms from the mean O1O2N1N2 plane of ±0.04 Å and an angle between the O1−Co−N1 and the O2−Co−N2 planes of ca. 3° both in $[\mathbf{1\text{-}im_2}]^+$ and in $[\mathbf{2\text{-}im_2}]^+$. Interestingly, we observed a slight asymmetry in the coordination bonds that may be at least partially due to the asymmetric positioning of the *N*-methylimidazole ligands in the molecule.

Vis−NIR spectra of $[\mathbf{1\text{-}im_2}]^+$ and $[\mathbf{2\text{-}im_2}]^+$ in CH_2Cl_2 are depicted in Figure 2. Spectra are dominated by bands at 444 (7550 M^{-1} cm^{-1}) and 416 nm (6340 M^{-1} cm^{-1}), respectively (Table 3). The principal electronic excitation that contributes to this band was assigned to a βHOMO−1 → βLUMO+2 transition ($\lambda_{\chi calcd}$ = 496 nm, f = 0.126 for $[\mathbf{1\text{-}im_2}]^+$ and $\lambda_{\chi calcd}$ = 433 nm, f = 0.082 for $[\mathbf{2\text{-}im_2}]^+$, Table 4) on the basis of TD-DFT calculations. The donor orbital is a delocalized π system involving both phenolate rings, while the acceptor orbital is a delocalized system involving both the salicylidene moieties and the metal (pure d_{z2} for $[\mathbf{1\text{-}im_2}]^+$, mixed d_{z2} and d_{xz} for $[\mathbf{2\text{-}im_2}]^+$) (Figure 4). Again, the energy of the transition is slightly overestimated in the calculation, but the trend in the energy of the transition $[\mathbf{1\text{-}im_2}]^+$ < $[\mathbf{2\text{-}im_2}]^+$ is well predicted.

Characterization of the One-Electron-Oxidized Complexes in CH_2Cl_2. Oxidation of the neutral complexes **1** and **2** in neat CH_2Cl_2 was realized by adding $AgSbF_6$ as one-electron oxidant to the medium. Indeed, air is not oxidizing enough to promote reaction under these conditions (see the electrochemical discussion). Diffusion of pentane into solutions of these complexes results in formation of single crystals of $[\mathbf{1\text{-}H_2O}](\mathbf{SbF_6})\cdot\mathbf{0.68\ H_2O}\cdot\mathbf{0.82CH_2Cl_2}$ and $[\mathbf{2\text{-}H_2O}](\mathbf{SbF_6})\cdot\mathbf{0.3H_2O}\cdot\mathbf{0.85CH_2Cl_2}$, which were subjected to X-ray diffraction. Crystals of $[\mathbf{1\text{-}H_2O}](\mathbf{SbF_6})\cdot\mathbf{0.68\ H_2O}\cdot\mathbf{0.82CH_2Cl_2}$ were of sufficient quality for detailed structural analysis, whereas crystals of $[\mathbf{2\text{-}H_2O}](\mathbf{SbF_6})\cdot\mathbf{0.3H_2O}\cdot\mathbf{0.85CH_2Cl_2}$ were not. Therefore, we will limit the discussion concerning $[\mathbf{2\text{-}H_2O}](\mathbf{SbF_6})\cdot\mathbf{0.3H_2O}\cdot\mathbf{0.85CH_2Cl_2}$ to general comments on its global structure (Supporting Information Figure S3).

In $[\mathbf{1\text{-}H_2O}](\mathbf{SbF_6})\cdot\mathbf{0.68\ H_2O}\cdot\mathbf{0.82CH_2Cl_2}$ the geometry of the metal ion is square pyramidal with an adventitious water molecule coordinated at the apical position at a Co−O3 bond distance 2.094(3) Å, with the O1, O2, N1, and N2 atoms occupying the equatorial positions. One hydrogen of the coordinated water molecule is H bonded to a second noncoordinating water molecule present in the crystal cell (O3−O6 bond distance of 2.573(8) Å, O3−H1−O6 angle of 159°). Close contacts exist between the H2 hydrogen of the coordinated water molecule and the F1 atom of the counterion (F1−O3 bond distance of 2.764(6) Å).

The atoms located in the N_2O_2 basal set are coplanar within 0.01 Å, and the cobalt ion is displaced by 0.130 Å above this mean plane and toward the O3 atom. The Co−O1, Co−O2, Co−N1, and Co−N2 bond distances are 1.850[2], 1.847[2], 1.884(3), and 1.870(3) Å. The Co−O bond lengths in $[\mathbf{1\text{-}H_2O}]^+$ are significantly shorter than those in $[\mathbf{1\text{-}im_2}]^+$, but they are almost identical to the ones measured for **1** (mean Co−O bond distance in **1** = 1.846(3) Å). It is noticeable that these Co−O bond lengths are shorter than those reported for square pyramidal organocobalt(III) salophen complexes involving an axial alkyl ligand (1.865−1.914 Å)[51] or square pyramidal cobalt(II) salen complexes (1.90 Å)[52] but close to those reported for the halide adduct of the Jacobsen catalyst (1.844 Å).[53] On the other hand, the equatorial Co−N bond lengths in $[\mathbf{1\text{-}H_2O}]^+$ are found to be intermediate between the ones

dx.doi.org/10.1021/ic300763t | Inorg. Chem. 2012, 51, 10557−10571

observed for $[\mathbf{1}\text{-}\mathbf{im_2}]^+$ and **1**. All data point to a different electronic structure for the metal ion in the two cations $[\mathbf{1}\text{-}\mathbf{H_2O}]^+$ and $[\mathbf{1}\text{-}\mathbf{im_2}]^+$. Accordingly, the cation $[\mathbf{1}\text{-}\mathbf{H_2O}]^+$ was found to be paramagnetic in solution, as judged by the large spectral range in its ^{1}H NMR spectrum.[21]

DFT calculations were undertaken on both $[\mathbf{1}\text{-}\mathbf{H_2O}]^+$ and $[\mathbf{2}\text{-}\mathbf{H_2O}]^+$ by considering singlet (low-spin Co(III)−phenolate complex), triplet (low-spin Co(II)−phenoxyl complex), and quintet (high-spin Co(II)−phenoxyl complex) spin states. As shown in Table 8 the bond distances calculated by geometry optimization on the triplet form $[\mathbf{1}\text{-}\mathbf{H_2O}]^+$ match those of the X-ray structure within 0.01 Å. The bond distances calculated for the singlet form diverge slightly, especially the Co−O ones, when compared to the experimental bond lengths (overestimated by 0.025 Å). The bond distances calculated for the quintet form are largely overestimated (+0.06 and +0.15 Å for the averaged Co−O and Co−N bonds, respectively). In addition, the triplet is found to be favored by 22.9 and 16.1 kcal mol^{-1} (for $[\mathbf{1}\text{-}\mathbf{H_2O}]^+$ and $[\mathbf{2}\text{-}\mathbf{H_2O}]^+$, respectively) over the singlet and 8.5 and 9.7 kcal mol^{-1} (for $[\mathbf{1}\text{-}\mathbf{H_2O}]^+$ and $[\mathbf{2}\text{-}\mathbf{H_2O}]^+$, respectively) over the quintet, which makes the diamagnetic form irrelevant. Therefore, on the basis of combined X-ray diffraction data and DFT calculations the cation is assigned as a paramagnetic radical species involving a rather low-spin cobalt ion. The individual contributions of the atoms to the spin population in the triplets $[\mathbf{1}\text{-}\mathbf{H_2O}]^+$ and $[\mathbf{2}\text{-}\mathbf{H_2O}]^+$ are summarized in Table 7. We found that more than 70% of the total spin density in the triplets $[\mathbf{1}\text{-}\mathbf{H_2O}]^+$ and $[\mathbf{2}\text{-}\mathbf{H_2O}]^+$ is localized on the metal, the remaining spin density being equally distributed within the phenoxyl moieties.[54] Regarding the quintets $[\mathbf{1}\text{-}\mathbf{H_2O}]^+$ and $[\mathbf{2}\text{-}\mathbf{H_2O}]^+$, 69% and 71%, respectively, of the total spin density is localized on the metal, the remaining spin density being mainly localized within the aromatic rings.

Table 7. Individual Contributions of the Atoms to the Spin Density in $[\mathbf{1}\text{-}\mathbf{H_2O}]^+$, $[\mathbf{2}\text{-}\mathbf{H_2O}]^+$, $[\mathbf{1}\text{-}\mathbf{im_2}]^{2+}$, and $[\mathbf{2}\text{-}\mathbf{im_2}]^{2+}$[a]

atom	$[\mathbf{1}\text{-}\mathbf{H_2O}]^+$[b]		$[\mathbf{2}\text{-}\mathbf{H_2O}]^+$[b]		$[\mathbf{1}\text{-}\mathbf{im_2}]^{2+}$	$[\mathbf{2}\text{-}\mathbf{im_2}]^{2+}$
Co	1.50	2.77	1.60	2.83	0.01	0.02
O1	0.09	0.19	0.10	0.24	0.00	0.01
O2	0.09	0.26	0.10	0.27	0.24	0.27
O3	0.04	0.05	0.05	0.03		
N1	0.01	0.08	0.02	0.11	0.00	0.00
N2	0.01	0.08	0.02	0.11	0.04	0.08
C1	0.00	0.00	0.00	0.00	0.00	0.00
C2	0.03	0.04	0.02	0.04	0.00	0.00
C4	0.06	0.04	0.04	0.06	0.00	0.00
C6	0.03	0.04	0.02	0.04	0.00	0.00
C13	0.00	0.03	0.00	0.02	0.10	0.06
C14	0.03	0.09	0.02	0.06	0.17	0.16
C16	0.06	0.11	0.04	0.09	0.22	0.26
C18	0.03	0.09	0.02	0.06	0.08	0.13

[a]Atom numbering used.

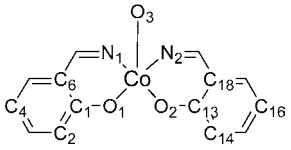

[b]First column: triplet form, second column: quintet form.

The two localized SOMOs of the triplets $[\mathbf{1}\text{-}\mathbf{H_2O}]^+$ and $[\mathbf{2}\text{-}\mathbf{H_2O}]^+$ are shown in Figure 6. For $[\mathbf{1}\text{-}\mathbf{H_2O}]^+$ one SOMO has a main metal character (82%), with small contributions of the coordinating atom of the ligands due to the covalency of the metal−ligand bonds. The second SOMO has mainly phenoxyl character (66%), with a contribution of 33% of the metal. The detailed analysis of the SOMOs thus points to a strong orbital mixing in $[\mathbf{1}\text{-}\mathbf{H_2O}]^+$, which confers to the cation a non-negligible ligand radical character. Consequently, $[\mathbf{1}\text{-}\mathbf{H_2O}]^+$ is best described by the three canonical structures shown in Scheme 2, with a larger weight for structure A.[18] Regarding $[\mathbf{2}\text{-}\mathbf{H_2O}]^+$, the composition of the first SOMO is again mainly metallic (87%), whereas the second one has both ligand (54%) and metal (45%) character. As for $[\mathbf{1}\text{-}\mathbf{H_2O}]^+$, DFT calculations

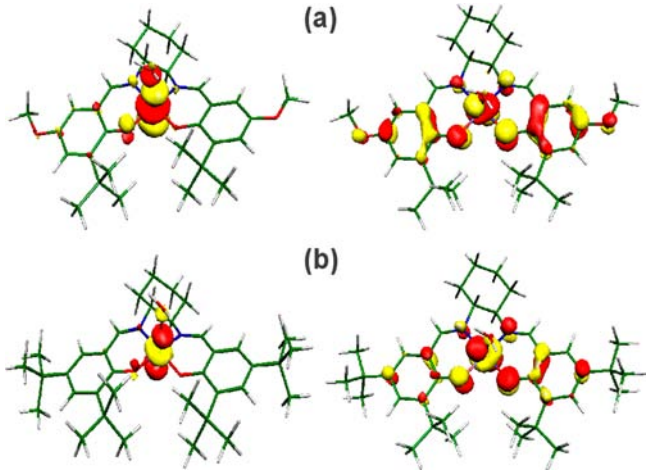

Figure 6. Localized SOMOs for the triplets (a) $[\mathbf{1}\text{-}\mathbf{H_2O}]^+$ and (b) $[\mathbf{2}\text{-}\mathbf{H_2O}]^+$.

Table 8. Comparison of Selected Experimental and Calculated Bond Lengths [Angstroms] for $[\mathbf{1}\text{-}\mathbf{H_2O}]^+$ and $[\mathbf{2}\text{-}\mathbf{H_2O}]^+$

bond	$[\mathbf{1}\text{-}\mathbf{H_2O}]$ (exp)	$[\mathbf{1}\text{-}\mathbf{H_2O}]^+$ (calcd)	$[\mathbf{1}\text{-}\mathbf{H_2O}]^+$ (calcd)	$[\mathbf{1}\text{-}\mathbf{H_2O}]^+$ (calcd)	$[\mathbf{2}\text{-}\mathbf{H_2O}]^+$ (calcd)	$[\mathbf{2}\text{-}\mathbf{H_2O}]^+$ (calcd)	$[\mathbf{2}\text{-}\mathbf{H_2O}]^+$ (calcd)
nature	triplet	triplet[b]	singlet[b]	quintet[b]	triplet[c]	singlet[c]	quintet[c]
Co−O1	1.849(2)	1.856	1.867	1.888	1.856	1.850	1.868
Co−O2	1.851(3)	1.845	1.872	1.925	1.856	1.857	1.882
Co−N1	1.880(4)	1.881	1.872	2.047	1.882	1.893	2.055
Co−N2	1.851(3)	1.881	1.880	2.060	1.888	1.911	2.055
Co−O3	2.082(4)	2.143	2.194	2.107	2.137	1.975	2.097
C1−O1	1.316(6)	1.312	1.302	1.308	1.316	1.319	1.310
C13−O2	1.320(5)	1.316	1.302	1.293	1.318	1.325	1.305

[a]In the crystals of $[\mathbf{1}\text{-}\mathbf{H_2O}](\mathbf{SbF_6})\cdot\mathbf{0.68\ H_2O}\cdot\mathbf{0.82CH_2Cl_2}$. [b]The triplet state is favored by 22.9 kcal mol^{-1} over the singlet state and 8.5 kcal mol^{-1} over the quintet state. [c]The triplet state is favored by 16.1 kcal mol^{-1} over the singlet state and 9.7 kcal mol^{-1} over the quintet state.

dx.doi.org/10.1021/ic300763t | Inorg. Chem. 2012, 51, 10557−10571

Scheme 2. Canonical Structures Describing the One-Electron-Oxidized Co(II) Complexes

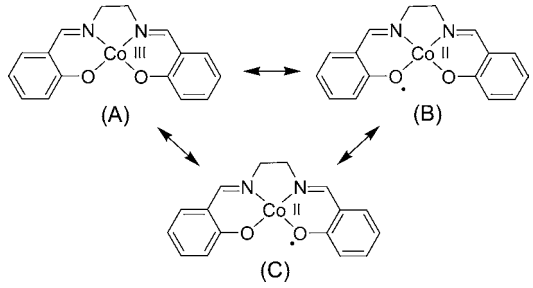

thus evidence a non-negligible contribution of the Co(II)-radical valence isomer in the case of $[\mathbf{2}\text{-}\mathbf{H_2O}]^+$, Figure 6. When compared to $[\mathbf{2}\text{-}\mathbf{H_2O}]^+$ the SOMO of $[\mathbf{1}\text{-}\mathbf{H_2O}]^+$ features an increased ligand (phenoxyl) contribution due to the enhanced electron-donating ability of the methoxy substituent, as observed in some nickel radical salen complexes.[55] The SOMOs of the quintets $[\mathbf{1}\text{-}\mathbf{H_2O}]^+$ and $[\mathbf{2}\text{-}\mathbf{H_2O}]^+$ are shown in Supporting Information Figures S14 and S15. For $[\mathbf{1}\text{-}\mathbf{H_2O}]^+$ two of the four SOMOs have main metal character (87% and 75%, which correspond mainly to d_{z2} and mixed $d_{x2-y2}-d_{xy}$ orbitals, respectively). The two other ones have significant phenoxyl character (45% and 43%), in addition to the metal character. For $[\mathbf{2}\text{-}\mathbf{H_2O}]^+$ three of the four SOMOs exhibit main metal character (83%, 80%, and 80%, which correspond to d_{z2}, d_{x2-y2}, and d_{xy} orbitals, respectively) whereas the fourth one has both phenoxyl (62%) and metal (38%) character. As for the triplets, DFT calculations thus highlight a significant contribution of the Co(II)-radical valence isomer in the electronic structure of the quintets.

Because the paramagnetic $[\mathbf{1}\text{-}\mathbf{H_2O}]^+$ (and $[\mathbf{2}\text{-}\mathbf{H_2O}]^+$) in frozen solution was found to be difficult to detect at the X-band frequency both at 10 and at 100 K, we run Q-band EPR experiments at 7 K on a powder sample. The 35 GHz spectrum displays a broad signal at $g \approx 5.3$ as well as a radical signal at $g \approx 2$ (Supporting Information Figure S5). This spectrum was found difficult to interpret by considering a triplet on the basis of the calculated zero-field splitting (ZFS) parameters for copper(II)−salen radical complexes.[6] We alternatively interpret it by considering a high-spin cobalt ion (S_{Co}= 3/2). For a high-spin Co(II) the ZFS parameters are much larger than the microwave energy and the doublet separation is too high to observe interdoublet transitions. Under this regime a signal corresponding to the allowed transition within the $|-1/2,+1/2\rangle$ doublet is observed at an effective g value lying within the range $5 < g_{eff} < 6$,[56] which matches quite well the experimental peak at $g \approx 5.8$. EPR spectroscopy thus suggests that $[\mathbf{1}\text{-}\mathbf{H_2O}]^+$ consists of a high-spin rather than low-spin Co(II) ion weakly interacting with a ligand radical. Additionally, a radical feature is observed on the spectrum with a strong signal centered at g = 2.

The discrepancy between EPR and crystallographic data, which suggest a low-spin Co(II)−phenoxyl radical character for $[\mathbf{1}\text{-}\mathbf{H_2O}]^+$, likely results from packing forces that can be strong enough to maintain a low-spin configuration in the crystals as well as the existence of a H-bond network, which may affect the nucleophilicity of the coordinating water molecule (a six-coordinate adduct may be also accessible). Noteworthy, both low- and high-spin configurations have been reported for square pyramidal cobalt(II) bis(phenolate) salen complexes.[52,57−61] For example, the monohydrate *N*,*N*′-ethylenebis-

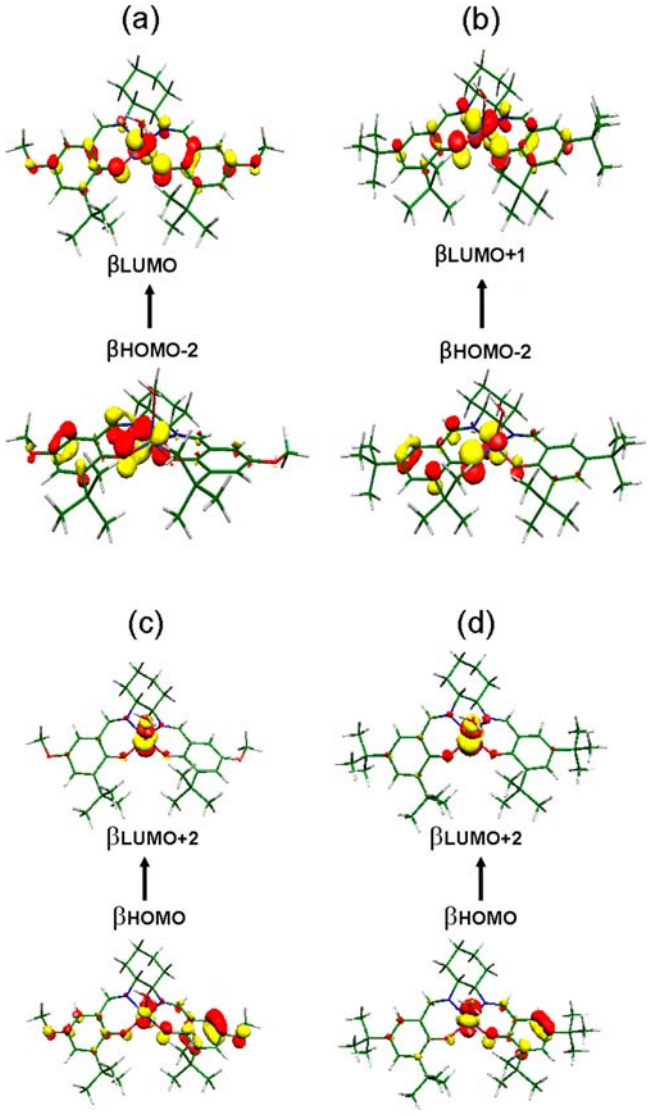

Figure 7. TD-DFT assignment of the lowest energy transition in (a) $[\mathbf{1}\text{-}\mathbf{H_2O}]^+$ (triplet), (b) $[\mathbf{2}\text{-}\mathbf{H_2O}]^+$ (triplet), (c) $[\mathbf{1}\text{-}\mathbf{H_2O}]^+$ (quintet), and (d) $[\mathbf{2}\text{-}\mathbf{H_2O}]^+$ (quintet).

(3-methoxysalicylidene-iminato)cobalt(II) complex was found to be high spin on the basis on magnetic measurements.[58] X-ray diffraction showed that the *N*-methylimidazole imidazole adduct of the *N*,*N*′-phenylenebis(salicylidene-iminato)cobalt-(II) complex was also high spin,[59] but the pyridine adduct of the *N*,*N*′-ethylenebis(salicylidene-iminato)cobalt(II) complex was low spin.[52] In order to confirm that the cation $[\mathbf{1}\text{-}\mathbf{H_2O}]^+$ is paramagnetic we measured the product of the magnetic susceptibility with temperature (χT) versus temperature on a powder sample of $[\mathbf{1}\text{-}\mathbf{H_2O}](\mathbf{SbF_6})\cdot\mathbf{0.68H_2O}\cdot\mathbf{0.82CH_2Cl_2}$ (Supporting Information Figure S6). At room temperature χT is 1.47 cm^3 K mol^{-1} and then decreases almost linearly upon cooling down to 50 K, where the decrease becomes more abrupt to reach almost zero at 2 K. The room-temperature value of χT is lower than the value (2.25 cm^3 K mol^{-1}) expected for one high-spin cobalt(II) (S = 3/2, $g \approx 2$, χT = 1.875 cm^3 K mol^{-1}) plus one radical (S = 1/2, g = 2, χT = 0.375 cm^3 K mol^{-1}) magnetically independent. It is however far above the value (0.75 cm^3 K mol^{-1}) expected for a low-spin cobalt(II) (S = 1/2, $g \approx 2$, χT = 0.375 cm^3 K mol^{-1}) plus one radical (S = 1/2; g = 2, χT = 0.375 cm^3 K mol^{-1}) without

dx.doi.org/10.1021/ic300763t | *Inorg. Chem.* 2012, 51, 10557−10571

considering any interaction. It is also too high if we consider a low-spin cobalt(II) ferromagnetically coupled with a radical at room temperature ($S = 1$, $\chi T = 1.0$ cm^3 K mol^{-1}). Thus, the thermal variation of χT better suggests that the cobalt(II) is high spin but strongly antiferromagnetically coupled with the phenoxyl radical giving a ground state spin $S = 1$ (if we consider a real spin $S = 3/2$ for the cobalt(II) ion). A survey of the literature shows that most magnetic studies of Co(II) complexes are concerned with four-coordinated cobalt(II) ions that are unambiguously low spin in a square planar geometry and high spin in a tetrahedral one. Six-coordinated cobalt(II) metal ions are always high spin.[62] As stated above there are fewer studies of five-coordinated cobalt(II) ions, which may be either high or low spin.[60,61] The trigonal bipyramidal environment results generally in a high-spin state,[60] but for square planar pyramids both situations are found.[61] Owing to the square pyramidal geometry of the cobalt ion in $[\mathbf{1}\text{-}\mathbf{H_2O}]^+$ the magnetic behavior is complicated by the low symmetry and spin−orbit coupling should be included to interpret the low-temperature behavior.[63] In order to estimate the correctness of the model and have an estimation of the strength of the interaction the magnetic susceptibility was tentatively simulated above 100 K by considering the spin Hamiltonian $H = -2JS_1S_2$ ($S_1 = 1/2$, $S_2 = 3/2$) and using the following equation

$$\chi T = \frac{Ng^2\beta^2[2 + 10\exp(4J/kT)]}{k[3 + 5\exp(4J/kT)]}$$

A good fit of the experimental data was obtained in the range 100−300 K with an antiferromagnetic coupling $J = -110.3$ cm^{-1} and $g = 2.11$, without considering intermolecular interaction. The whole set of data may be well fitted considering this model with $J = -138.9$ cm^{-1}, $g = 2.29$, plus intermolecular interaction $\theta = -19$ cm^{-1}. However, this result is only indicative since a more rigorous model including spin−orbit effect should be used here, as pointed out above. Noteworthy, attempts to fit the data by considering intermolecular antiferromagnetic interactions in between a ($S = 1$) system corresponding to a low-spin cobalt(II) antiferromagnetically coupled with a phenoxyl radical at room temperature were unsuccessful.

Therefore, our X-ray diffraction, EPR, and magnetic susceptibility data are all consistent with a phenoxyl radical character for $[\mathbf{1}\text{-}\mathbf{H_2O}]^+$.

Vis−NIR spectra of $[\mathbf{1}\text{-}\mathbf{H_2O}]^+$ and $[\mathbf{2}\text{-}\mathbf{H_2O}]^+$ are depicted in Figure 3. Both cations absorb significantly over the entire visible region, similarly to the analogous nickel radical salen complexes[8] and cobalt−iminosemiquinonate radical complexes.[18−20] Most importantly, both $[\mathbf{1}\text{-}\mathbf{H_2O}]^+$ and $[\mathbf{2}\text{-}\mathbf{H_2O}]^+$ exhibit a remarkable NIR feature at 1220 (7370 M^{-1} cm^{-1}) and 1060 nm (5560 M^{-1} cm^{-1}), respectively. It is important to note that neither **1** or $[\mathbf{1}\text{-}\mathbf{im_2}]^+$ nor **2** or $[\mathbf{2}\text{-}\mathbf{im_2}]^+$ exhibits a band in the NIR region (Table 3). On the basis of its high intensity, this band cannot originate from a d−d transition; therefore, it is ascribed to a CT transition. In addition, its low energy is indicative of a small energy gap between the ground and the excited states, whose nature was investigated by time-dependent DFT calculations.

The absence of intense NIR transitions for **1** and $[\mathbf{1}\text{-}\mathbf{im_2}]^+$ (as well as **2** and $[\mathbf{2}\text{-}\mathbf{im_2}]^+$) is well predicted, whereas an electronic excitation could be calculated in the NIR region for both $[\mathbf{1}\text{-}\mathbf{H_2O}]^+$ and $[\mathbf{2}\text{-}\mathbf{H_2O}]^+$. Noteworthy, the NIR band is predicted by considering both low-spin Co(II)−phenoxyl and high-spin Co(II)−phenoxyl complexes, but its origin differs. By considering a low-spin Co(II)−phenoxyl configuration it corresponds to a βHOMO−2→ βLUMO transition in the case of $[\mathbf{1}\text{-}\mathbf{H_2O}]^+$, while it is a βHOMO−2 → βLUMO+1 transition in $[\mathbf{2}\text{-}\mathbf{H_2O}]^+$. The predicted energies are 1013 (f = 0.110) and 952 nm (f = 0.158) for $[\mathbf{1}\text{-}\mathbf{H_2O}]^+$ and $[\mathbf{2}\text{-}\mathbf{H_2O}]^+$, respectively, which is in fairly good agreement with the experimental bands (1217 and 1060 nm, respectively). The composition of the donor orbital is a delocalized π system involving one aromatic ring and a d_{yz} metal orbital in both cases. The acceptor orbital is a delocalized π system involving two aromatic rings and a metal orbital that mainly has d_{z2} (for $[\mathbf{1}\text{-}\mathbf{H_2O}]^+$) or d_{yz} character (for $[\mathbf{2}\text{-}\mathbf{H_2O}]^+$). By considering a high-spin Co(II)−phenoxyl system the NIR band arises from a βHOMO → βLUMO+2 transition for both $[\mathbf{1}\text{-}\mathbf{H_2O}]^+$ and $[\mathbf{2}\text{-}\mathbf{H_2O}]^+$. The transition is mainly a ligand-to-metal CT transition: The donor orbital is a delocalized π system involving the aromatic rings (with a larger contribution of the phenolate ring) and a d_{xz} metal orbital, while the acceptor one has d_{z2} character. The predicted energies are 1183 (f = 0.210) and 1154 nm (f = 0.103) for $[\mathbf{1}\text{-}\mathbf{H_2O}]^+$ and $[\mathbf{2}\text{-}\mathbf{H_2O}]^+$, respectively. Although these values are in better agreement with the experimental data, the difference in the calculated bands by considering low- and high-spin Co(II)-phenoxyl species is relatively small and it is not possible to conclude unambiguously on the metal ion spin state in the radicals $[\mathbf{1}\text{-}\mathbf{H_2O}]^+$ and $[\mathbf{2}\text{-}\mathbf{H_2O}]^+$ in solution.

Characterization of the Two-Electron-Oxidized Complexes in CH_2Cl_2. The two-electron-oxidized forms of complexes **1** and **2** were generated electrochemically in CH_2Cl_2 at low temperature (240 K) due to their limited stability. UV−vis spectra of the dications $[\mathbf{1}]^{2+}$ and $[\mathbf{2}]^{2+}$ in CH_2Cl_2 (+0.01 M TBAP) at 240 K are depicted in Figure 8.

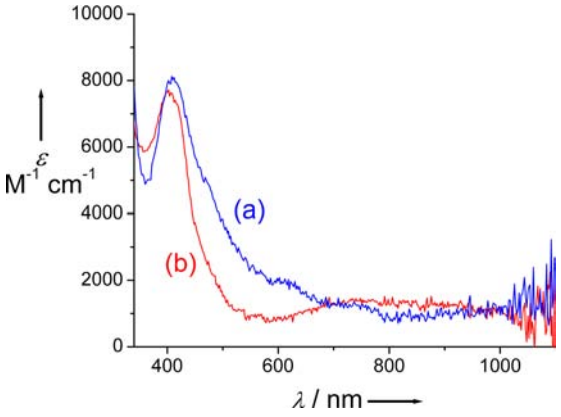

Figure 8. UV−vis spectra of the electrochemically generated dications in 0.05 mM CH_2Cl_2 solutions (+0.01 M TBAP): (a) $[\mathbf{1}]^{2+}$ (blue) nd (b) $[\mathbf{2}]^{2+}$ (red). T = 240 K.

They are dominated by bands at 408 (8120 M^{-1} cm^{-1}) and 402 nm (7720 M^{-1} cm^{-1}) for $[\mathbf{1}]^{2+}$ and $[\mathbf{2}]^{2+}$, respectively. An additional broad band of weaker intensity could be observed at 800 nm (ε = 1420 M^{-1} cm^{-1}) in the spectrum of $[\mathbf{2}]^{2+}$. These spectral features match remarkably well those reported for phenoxyl−Co(III)[11,64] and phenoxyl−Cu(II)[65] complexes generated from Mannich bases. The dications thus comprise a phenoxyl radical moiety coordinated to a genuine Co(III) metal ion. Addition of *N*-methylimidazole (10 equiv) to the

dx.doi.org/10.1021/ic300763t | Inorg. Chem. 2012, 51, 10557−10571

CH_2Cl_2 solution of $[\mathbf{1}]^{2+}$ and $[\mathbf{2}]^{2+}$ results in a gradual decrease of the intensity of the spectra, without significant shift of the bands. This indicates that the dications are poorly stable in the presence of *N*-methylimidazole.

The X-band EPR spectra of the dications $[\mathbf{1}]^{2+}$ and $[\mathbf{2}]^{2+}$ in CH_2Cl_2 (+0.1 M TBAP) solution are shown in Figure 9. Both

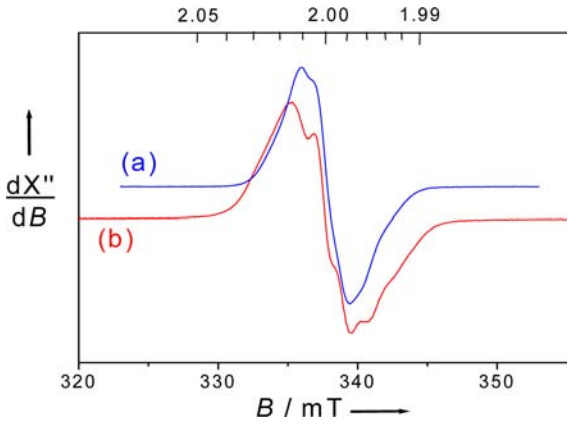

Figure 9. X-band EPR spectra of the electrochemically generated dications (a) $[\mathbf{1}]^{2+}$ and (b) $[\mathbf{2}]^{2+}$ in 0.5 mM CH_2Cl_2 (+0.1 M TBAP) solution. Microwave frequency: 9.45 GHz. Power: 5.5 mW. Mod. amp. 0.1 mT. Frequency: 100 kHz. T = 100 K.

spectra consist of an S = 1/2 signal centered at g_{iso} = 2.00. This behavior is clear evidence for the presence of a phenoxyl radical coordinated to a low-spin Co(III) metal ion as similar g values (lower than the one of the free electron 2.0023) were reported for Co(III)−phenoxyl radical species.[10,11,64] This assignment is confirmed by the observation of a hyperfine interaction of the electron spin with the cobalt nucleus which splits the EPR signal. Because the hyperfine coupling constants are within of range of the line width the splitting could be mainly observed as shoulders in the S = 1/2 peak. It is worth noting that the signal is highly isotropic without any hyperfine coupling constant higher than 100 MHz. Van Doorslaer et al. showed that this behavior is indicative of an octahedral geometry for the metal ion, the calculated g values for pentacoordinated cobalt(III) radical complexes being less than 2.00 with stronger hyperfine coupling constants.[10] In addition, the signal is found to be distributed over a larger spectral width when $[\mathbf{2}]^{2+}$ is compared to $[\mathbf{1}]^{2+}$. That may suggest that the ligand radical spin interacts more strongly with the Co(III) nuclear spin in the case of $[\mathbf{2}]^{2+}$.

EPR spectra were recorded just after addition of 10 equiv of *N*-methylimidazole to a CH_2Cl_2 solution of the electrogenerated dication. A strong decrease of intensity was observed, consistent with fast decomposition of the dication. The EPR signal resembles those of $[\mathbf{1}]^{2+}$ and $[\mathbf{2}]^{2+}$ in CH_2Cl_2, but they are not superimposable. This confirms that *N*-methylimidazole coordinates to the metal center before decomposition, affording the octahedral low-spin Co(III) complexes $[\mathbf{1}\text{-}\mathbf{im}_2]^{2+}$ and $[\mathbf{2}\text{-}\mathbf{im}_2]^{2+}$.[10] The fact that only slight changes arise from addition of *N*-methylimidazole to the CH_2Cl_2 solution of the dications further confirms that the Co(III) ion likely already adopts an octahedral geometry both in $[\mathbf{1}]^{2+}$ and in $[\mathbf{2}]^{2+}$.

On the basis of our EPR results, DFT calculations were undertaken on $[\mathbf{1}\text{-}\mathbf{im}_2]^{2+}$ and $[\mathbf{2}\text{-}\mathbf{im}_2]^{2+}$ by considering a S = 1/2 ground spin state and two axially bound *N*-methylimidazoles. Geometry optimization reveals that the equatorial coordinating atoms deviate by ±0.04 Å from the mean O1,O2,N1,N2 plane. In addition, the angle between the two O1−Co−N1 and O2−Co−N2 planes is ca. 4° both in $[\mathbf{1}\text{-}\mathbf{im}_2]^{2+}$ and in $[\mathbf{2}\text{-}\mathbf{im}_2]^{2+}$. These geometrical features compare quite well with those calculated for the monocations $[\mathbf{1}\text{-}\mathbf{im}_2]^{+}$ and $[\mathbf{2}\text{-}\mathbf{im}_2]^{+}$. Nevertheless, examination of the coordination bond lengths reveals a strong asymmetry in the C−O bond distances (Table 9): The Co−O1 bond length is 1.962 Å, while

Table 9. Calculated Bond Lengths [Angstroms] for the Dications

bond	$[\mathbf{1}]^{2+}$	$[\mathbf{1}\text{-}\mathbf{im}_2]^{2+}$	$[\mathbf{2}]^{2+}$	$[\mathbf{2}\text{-}\mathbf{im}_2]^{2+}$
Co−O1	1.962	1.977	1.968	1.978
Co−O2	1.893	1.911	1.893	1.912
Co−N1	1.931	1.937	1.933	1.933
Co−N2	1.898	1.907	1.896	1.903
Co−Ax 1[a]	1.956	1.985	1.955	1.985
Co−Ax 2[a]	1.959	2.002	1.955	2.001
C1−O1	1.274	1.270	1.272	1.268
C13−O2	1.323	1.316	1.322	1.311

[a]Coaxial bonds: Co−Ax 1 corresponds to Co−N3 and Co−Ax 2 corresponds to Co−N4 for $[\mathbf{1}\text{-}\mathbf{im}_2]^{2+}$ and $[\mathbf{2}\text{-}\mathbf{im}_2]^{2+}$. Co−Ax 1 corresponds to Co−O3 and Co−Ax 2 corresponds to Co−O4 for $[\mathbf{1}]^{2+}$ and $[\mathbf{2}]^{2+}$.

the Co−O2 one is 1.893 Å. These values differ significantly from the ones calculated for the monocation $[\mathbf{1}\text{-}\mathbf{im}_2]^{2+}$ (1.914 and 1.905 Å). Such asymmetry is indicative of phenoxyl radical localization on a single aromatic ring (the one bearing the O1 atom).[6] This assumption is confirmed by the quinonoid distribution of bond length within one ring with C1−O1, C1−C2, C2−C3, C3−C4, C4−C5, C5−C6, and C1−C6 bond distances of 1.270, 1.468, 1.376, 1.411, 1.409, 1.376, and 1.456 Å, the corresponding bond distances in the other ring being 1.316, 1.435, 1.391, 1.405, 1.375, 1.411, and 1.429 Å (atom numbering is indicated in Table 7). Similar behavior is observed for $[\mathbf{2}\text{-}\mathbf{im}_2]^{2+}$. Not surprisingly, the SOMO is almost exclusively distributed on a single phenoxyl ring in both $[\mathbf{1}\text{-}\mathbf{im}_2]^{2+}$ and $[\mathbf{2}\text{-}\mathbf{im}_2]^{2+}$, Figure 10. Both $[\mathbf{1}\text{-}\mathbf{im}_2]^{2+}$ and $[\mathbf{2}\text{-}\mathbf{im}_2]^{2+}$ are thus localized phenoxyl−Co(III) complexes.

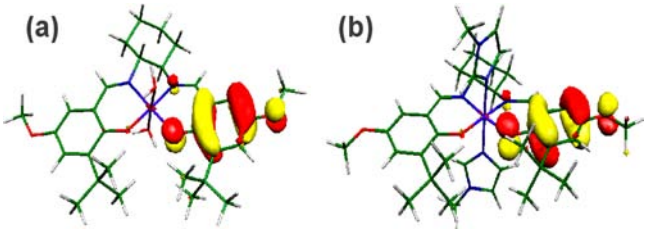

Figure 10. Localized SOMOs for (a) $[\mathbf{1}]^{2+}$ and (b) $[\mathbf{1}\text{-}\mathbf{im}_2]^{2+}$.

Regarding $[\mathbf{1}]^{2+}$ and $[\mathbf{2}]^{2+}$, we performed DFT calculations by considering a hexacoordinated cobalt ion, with two water molecules occupying the axial positions in the metal coordination sphere.[66] From geometry optimization it appears that the overall geometry of the complex is hardly affected by the nature of the axial ligands, the coordination sphere being somewhat slightly more contracted in $[\mathbf{1}]^{2+}$ and $[\mathbf{2}]^{2+}$ than in $[\mathbf{1}\text{-}\mathbf{im}_2]^{2+}$ and $[\mathbf{2}\text{-}\mathbf{im}_2]^{2+}$ (Table 9). The composition of the SOMO is again ligand centered and exclusively distributed on a single phenoxyl ring (more than 90%).

dx.doi.org/10.1021/ic300763t | *Inorg. Chem.* 2012, 51, 10557−10571

DFT studies show that the dications are localized phenoxyl−Co(III) complexes irrespective of the phenol substituent and axial ligand, in agreement with recent work published by Van Doorslaer et al.[10] It is noteworthy that the small electronic coupling between the two redox-active rings is also evident from electrochemical studies. Indeed, the $\Delta E_{1/2} = E_{1/2}{}^{3} - E_{1/2}{}^{2}$ value is very low in both **1** and **2**, consistent very poor electrochemical communication between the phenoxyl and the phenolate moieties. The systematic ligand radical localization in this series contrasts with the results obtained for the nickel(II) salen radical complexes,[6,7e] where the *tert*-butyl groups promote ligand radical delocalization (the SOMO is shared between the two rings) and more electron-donating groups like OMe induce ligand radical localization. The behavior observed for the cobalt salen complexes is more in line with the recent results obtained by Fujii et al.[67] on manganese salen radical complexes. They showed that a nickel to manganese substitution drastically limits electron transfer between the two redox centers (phenolate and phenoxyl) and that manganese−salen radical complexes exhibit a localized phenoxyl character. Modulation of the redox potential of the electron donor and acceptor relative to the metal ion mediator was proposed to account for the resulting ligand radical localization. Noteworthy, the Co(III) metal ion exhibits a similar formal charge to the Mn(III) ion and an increase in the metal charge is expected to increase the phenoxyl/phenolate oxidation potential. This expectation is experimentally verified, with formation of the Co(III)−phenoxyl species occurring at 0.49 and 0.65 V for $[\mathbf{1}]^{2+}$ and $[\mathbf{2}]^{2+}$, respectively, versus 0.22 and 0.37 V for the corresponding Ni(II)−phenoxyl complex.

A higher metal charge thus significantly alters the ligand radical delocalization in this series, providing a localized radical character for the Co(III) salen complexes.

CONCLUSION

The present study unambiguously shows that the electronic structure of one-electron-oxidized square planar cobalt(II)−salen complexes strongly depends on the medium. Cations $[\mathbf{1}\text{-}\mathbf{H_2O}]^{+}$ and $[\mathbf{2}\text{-}\mathbf{H_2O}]^{+}$ were generated by silver oxidation in neat CH_2Cl_2 (air is not powerful enough under these conditions). Adventitious water coordinates to the metal ion in the absence of a strong donor in solution. Cations $[\mathbf{1}\text{-}\mathbf{H_2O}]^{+}$ and $[\mathbf{2}\text{-}\mathbf{H_2O}]^{+}$ are consequently not square planar like their neutral precursor but square pyramidal with a water molecule coordinated at the apical position. These species may constitute crucial intermediates in the catalytic ring opening of epoxides. It should be underlined that the catalytic opening of epoxide is believed to occur by a cooperative bimetallic mechanism involving a square pyramidal Co(III) complex containing an axially bound nucleophile, which attacks an epoxide substrate coordinated to a second octahedral Co(III) complex.[13,21] The best catalytic system involves one-electron-oxidized **2** as an equimolar mixture of Cl^- and SbF_6^- adducts in the presence a small amount of water. A key step in the reaction is attack of the nucleophile (hydroxyl group) on the epoxide. Formation of this nucleophile is proposed to result from binding of water on the counterion adduct of **2** and deprotonation due to the Lewis acidity of the cobalt(III) ion. The high-resolution structure of $[\mathbf{1}\text{-}\mathbf{H_2O}]^{+}$ and the general arrangement of $[\mathbf{2}\text{-}\mathbf{H_2O}]^{+}$ provide the first evidence for the absence of ligation of the SbF_6^- anion. Instead, the SbF_6^- adduct of the Jacobsen catalyst $[\mathbf{2}\text{-}\mathbf{H_2O}]^{+}$ probably already contains the nucleophile precursor (water molecule) coordinated to the square pyramidal metal ion, which may explain the high rates obtained when this complex is used for ring opening of epoxides. Both $[\mathbf{1}\text{-}\mathbf{H_2O}]^{+}$ and $[\mathbf{2}\text{-}\mathbf{H_2O}]^{+}$ exhibit a paramagnetic ($S = 1$) ground spin state, with the spin density being mainly localized on the metal. Importantly, the remaining spin density is distributed over the aromatic rings, showing that the cations have a non-negligible phenoxyl character never evidenced previously. Both $[\mathbf{1}\text{-}\mathbf{H_2O}]^{+}$ and $[\mathbf{2}\text{-}\mathbf{H_2O}]^{+}$ exhibit a remarkable NIR band at 1220 (7370 M^{-1} cm^{-1}) and 1060 nm (5560 M^{-1} cm^{-1}), respectively, assigned to CT transition. Preliminary DFT calculations were undertaken on structures derived from $[\mathbf{1}\text{-}\mathbf{H_2O}]^{+}$ and $[\mathbf{2}\text{-}\mathbf{H_2O}]^{+}$ with the water molecule being substituted by an acetate anion. They highlight a dramatic effect of ligand charge upon electronic structure (paramagnetic Co(III)−bis(phenolate) cation in this case) that will be further investigated.[54] In the presence of *N*-methylimidazole, **1** and **2** are easily oxidized by air into the genuine octahedral cobalt(III) bis(phenolate) complexes $[\mathbf{1}\text{-}\mathbf{im_2}]^{+}$ and $[\mathbf{2}\text{-}\mathbf{im_2}]^{+}$. Neither $[\mathbf{1}\text{-}\mathbf{im_2}]^{+}$ nor $[\mathbf{2}\text{-}\mathbf{im_2}]^{+}$ exhibits a NIR band in its electronic spectrum. The NIR feature of $[\mathbf{1}\text{-}\mathbf{H_2O}]^{+}$ and $[\mathbf{2}\text{-}\mathbf{H_2O}]^{+}$ could be a spectroscopic marker for a ligand contribution to the electronic structure of the cations. The number and nature of the axial ligands and thus the external medium therefore play a crucial role in the stabilization of the Co(III)−L vs spin-coupled Co(II)−$L^{\bullet}$ valence isomer. The electrochemically generated dications $[\mathbf{1}]^{2+}$ and $[\mathbf{2}]^{2+}$ were identified as paramagnetic ($S = 1/2$) Co(III)−phenoxyl species by a characteristic absorption band at ca. 400 nm in the UV−vis spectrum and a highly isotropic EPR signal centered at $g = 2.00$. DFT studies show that both $[\mathbf{1}]^{2+}$ and $[\mathbf{2}]^{2+}$ are localized phenoxyl−Co(III) complexes, in agreement with recent work published by Van Doorslaer et al. on a derivative of $[\mathbf{2}]^{2+}$.[10] The present study shows that ligand radical localization occurs irrespective of the phenol substituent. This trend contrasts with the results obtained for the nickel(II) salen radical complexes in which *tert*-butyl groups promote ligand radical delocalization (the SOMO is shared between the two rings), whereas more electron-donating groups like OMe induce ligand radical localization. The behavior observed for phenoxyl−Co(III) complex resembles more that reported for phenoxyl−Mn(III) complexes by Fujii et al.[67] They nicely showed that a nickel to manganese substitution in radical salen complexes drastically limits electron transfer between the two redox centers (phenolate and phenoxyl), resulting in radical localization. A shift of the redox potential of the electron donor and acceptor relative to the metal ion mediator was proposed to account for the resulting ligand radical localization. The metal charge influences both the phenoxyl/phenolate oxidation potential and the metal ion geometry. The potential values corresponding to formation of $[\mathbf{1}]^{2+}$ and $[\mathbf{2}]^{2+}$ are almost similar to those reported for oxidation of the corresponding Mn(III)−phenolate complexes into Mn(III)−phenoxyl species, with an identical speculated geometry for the metal ion. These homologies may be responsible for the localized ligand radical character of the dications. Further studies are in progress in our laboratory to better understand the parameters involved in stabilization of the high-spin Co(III)−L vs spin-coupled Co(II)−$L^{\bullet}$ valence isomer.

ASSOCIATED CONTENT

Supporting Information

EPR spectra of **1**, $[\mathbf{1}\text{-}\mathbf{im_2}]^{2+}$, $[\mathbf{2}\text{-}\mathbf{im_2}]^{2+}$, and the superoxo/*N*-methylimidazole adducts of **1** and **2**; localized SOMOs for **1**, **2**,

$[\mathbf{1}]^{2+}$, and $[\mathbf{1}\text{-}\mathbf{im_2}]^{2+}$; spin density plots of $[\mathbf{1}\text{-}\mathbf{H_2O}]^{+}$, $[\mathbf{2}\text{-}\mathbf{H_2O}]^{+}$, and their water-to-acetate-substituted analogs; metrical parameters issued from geometry optimization for all complexes; TD-DFT assignment of the lowest energy transition in **2** and $[\mathbf{2}\text{-}\mathbf{im_2}]^{+}$. This material is available free of charge via the Internet at http://pubs.acs.org.

AUTHOR INFORMATION

Corresponding Author

*E-mail: fabrice.thomas@ujf-grenoble.fr.

Notes

The authors declare no competing financial interest.

ACKNOWLEDGMENTS

This work was supported by a doctoral fellowship (A.K.) from the DCM.

REFERENCES

(1) (a) Whittaker, J. W. In *Metal Ions in Biological Systems*; Sigel, H., Sigel, A., Eds.; Marcel Dekker: New York, 1994; Vol. *30*, p 315. (b) Borman, C. D.; Saysell, C. G.; Sokolowski, A.; Twitchett, M. B.; Wright, C.; Sykes, A. G. *Coord. Chem. Rev.* **1999**, *190*−*192*, 771. (c) McPherson, M. J.; Parsons, M. R.; Spooner, R. K.; Wilmot, C. M. In *Handbook for metalloproteins*; Messerschmidt, A., Huber, R., Poulos, T., Wieghardt, K., Eds.; John Wiley and Sons: New York, 2001; Vol. *2*, p 1272. (d) Whittaker, J. W. In *Advances in Protein Chemistry*; Richards, F. M., Eisenberg, D. S., Kuriyan, J., Eds.; Academic Press, Elsevier: New York, 2002; Vol. *60*, p 1. (e) Whittaker, J. W. *Chem. Rev.* **2003**, *103*, 2347. (f) Rogers, M. S.; Dooley, D. M. *Curr. Opin. Chem. Biol.* **2003**, *7*, 189. (g) Firbank, S. J.; Rogers, M.; Hurtado-Guerrero, R.; Dooley, D. M.; Halcrow, M. A.; Phillips, S. E. V.; Knowles, P. F.; McPherson, M. J. *Biochem. Soc. Trans.* **2003**, *31*, 506.

(2) Gordon, A.; Hamilton, G. A.; Adolf, P. K.; de Jersey, J.; DuBois, G. C.; Dyrkacz, G. R.; Libby, R. D. *J. Am. Chem. Soc.* **1978**, *100*, 1899.

(3) (a) Whittaker, M. M.; Whittaker, J. W. *J. Biol. Chem.* **1988**, *263*, 6074. (b) Babcock, G. T.; El-Deeb, M. K.; Sandusky, P. O.; Whittaker, M. M.; Whittaker, J. W. *J. Am. Chem. Soc.* **1992**, *114*, 3121. (c) McGlashen, M. L.; Eads, D. D.; Spiro, T. G.; Whittaker, J. W. *J. Phys. Chem.* **1995**, *99*, 4918. (d) Whittaker, M. M.; Ekberg, C. A.; Peterson, J.; Sendova, M. S.; Day, E. P.; Whittaker, J. W. *J. Mol. Catal. B: Enzym.* **2000**, *8*, 3.

(4) (a) Jazdzewski, B. A.; Tolman, W. B. *Coord. Chem. Rev.* **2000**, *200*−*202*, 633. (b) Krüger, H. J. *Angew. Chem., Int. Ed.* **1999**, *38*, 627. (c) Itoh, S.; Taki, M.; Fukuzumi, S. *Coord. Chem. Rev.* **2000**, *198*, 3. (d) Chaudhuri, P.; Wieghardt, K. *Prog. Inorg. Chem.* **2001**, *50*, 151. (e) Thomas, F. *Eur. J. Inorg. Chem.* **2007**, 2379. (f) Thomas, F. In *Stable Radicals: Fundamentals and Applied Aspects of Odd-Electron Compounds*; Hicks, R. G., Ed.; John Wiley and Sons: Chichester, 2010;pp 281.

(5) (a) Pratt, R. C.; Stack, T. D. P. *J. Am. Chem. Soc.* **2003**, *125*, 8716. (b) Pratt, R. C.; Stack, T. D. P. *Inorg. Chem.* **2005**, *44*, 2367. (c) Thomas, F.; Jarjayes, O.; Duboc, C.; Philouze, C.; Saint-Aman, E.; Pierre, J.-L. *Dalton Trans.* **2004**, 2662. (d) Storr, T.; Verma, P.; Pratt, R. C.; Wasinger, E. C.; Shimazaki, Y.; Stack, T. D. P. *J. Am. Chem. Soc.* **2008**, *130*, 15448.

(6) Orio, M.; Jarjayes, O.; Kanso, H.; Philouze, C.; Neese, F.; Thomas, F. *Angew. Chem., Int. Ed.* **2010**, *49*, 4989.

(7) (a) Shimazaki, Y.; Tani, F.; Fukui, K.; Naruta, Y.; Yamauchi, O. *J. Am. Chem. Soc.* **2003**, *125*, 10512. (b) Rotthaus, O.; Jarjayes, O.; Thomas, F.; Philouze, C.; Del Valle, C. P.; Saint-Aman, E.; Pierre, J. L. *Chem.*−*Eur. J* **2006**, *12*, 2293. (c) Rotthaus, O.; Thomas, F.; Jarjayes, O.; Philouze, C.; Saint-Aman, E.; Pierre, J. L. *Chem.*−*Eur. J* **2006**, *12*, 6953. (d) Shimazaki, Y.; Yajima, T.; Tani, F.; Karasawa, S.; Fukui, K.; Naruta, Y.; Yamauchi, O. *J. Am. Chem. Soc.* **2007**, *129*, 2559. (e) Storr, T.; Wasinger, E. C.; Pratt, R. C.; Stack, T. D. P. *Angew. Chem., Int. Ed.* **2007**, *46*, 5198. (f) Benisvy, L.; Kannappan, R.; Song, Y. F.; Milikisyants, S.; Huber, M.; Mutikainen, I.; Turpeinen, U.; Garnez, P.; Bernasconi, L.; Baerends, E. J.; Hartl, F.; Reedijk, J. *Eur. J. Inorg. Chem.* **2007**, 631. (g) Rotthaus, O.; Labet, V.; Philouze, C.; Jarjayes, O.; Thomas, F. *Eur. J. Inorg. Chem.* **2008**, 4215. (h) Rotthaus, O.; Jarjayes, O.; Philouze, C.; Del Valle, C. P.; Thomas, F. *Dalton Trans.* **2009**, 1792. (i) Shimazaki, Y.; Stack, T. D. P.; Storr, T. *Inorg. Chem.* **2009**, *48*, 8383. (j) Storr, T.; Verma, P.; Shimazaki, Y.; Wasinger, E. C.; Stack, T. D. P. *Chem.*−*Eur. J* **2010**, *16*, 8980. (k) Kochem, A.; Orio, M.; Jarjayes, O.; Neese, F.; Thomas, F. *Chem. Commun.* **2010**, *46*, 6765. (l) Dunn, T. J.; Ramogida, C. F.; Simmonds, C.; Paterson, A.; Wong, E. W. Y.; Chiang, L.; Shimazaki, Y.; Storr, T. *Inorg. Chem.* **2011**, *50*, 6746. (m) Shimazaki, Y.; Arai, N.; Dunn, T. J.; Yajima, T.; Tani, F.; Ramogida, C. F.; Storr, T. *Dalton Trans.* **2011**, *40*, 2469. (n) Verma, P.; Pratt, R. C.; Storr, T.; Wasinger, E. C.; Stack, T. D. P. *Proc. Natl. Acad. Sci. U.S.A.* **2011**, *108*, 18600.

(8) (a) Rotthaus, O.; Jarjayes, O.; Thomas, F.; Philouze, C.; Saint-Aman, E.; Pierre, J.-L. *Dalton Trans.* **2007**, 889. (b) Orio, M.; Philouze, C.; Jarjayes, O.; Neese, F.; Thomas, F. *Inorg. Chem.* **2010**, *49*, 646.

(9) (a) Neirn, A. K.; Bhalla, R.; Foxon, S. P.; Liu, X.; Yellowlees, L. J.; Gilbert, B. C.; Walton, P. H. *J. Chem. Soc., Dalton Trans.* **2002**, 1253. (b) Imbert, C.; Hratchian, H. P.; Lanznaster, M.; Heeg, M. J.; Hryhorczuk; McGarvey, B. R.; Schlegel, H. B.; Verani, C. N. *Inorg. Chem.* **2005**, *44*, 7414. (c) Floquet, S.; Ottenwaelder, X.; Boillot, M.-L. *Inorg. Chem. Commun.* **2007**, *10*, 1549. (d) Takuya Kurahashi, T.; Kobayashi, Y.; Nagatomo, S.; Tosha, T.; Kitagawa, T.; Fujii, H. *Inorg. Chem.* **2008**, *47*, 6804.

(10) (a) Vinck, E.; Murphy, D. M.; Fallis, I. A.; Van Doorslaer, S. *Appl. Magn. Reson.* **2010**, *37*, 289. (b) Vinck, E.; Murphy, D. M.; Fallis, I. A.; Strevens, R. R.; Van Doorslaer, S. *Inorg. Chem.* **2010**, *49*, 2083.

(11) Thomas, F.; Arora, H.; Philouze, C.; Jarjayes, O. *Inorg. Chim. Acta* **2010**, *363*, 3122.

(12) (a) Cozzi, P. G. *Chem. Soc. Rev.* **2004**, *33*, 410. (b) Zulauf, A.; Mellah, M.; Hong, X.; Schulz, E. *Dalton Trans.* **2010**, *39*, 6911.

(13) (a) Furrow, M. E.; Schauss, S. E.; Jacobsen, E. N. *J. Org. Chem.* **1998**, 6776. (b) Schaus, S. E.; Brandes, B. D.; Larrow, J. F.; Tokunaga, M.; Hansen, K. B.; Goult, A. E.; Furrow, M. E.; Jacobsen, E. N. *J. Am. Chem. Soc.* **2002**, *124*, 1307. (c) White, D. E.; Jacobsen, E. N. *Tetrahedron: Asymmetry* **2003**, *14*, 3633. (d) Nielsen, L. P. C.; Stevenson, C. P.; Blackmond, D. G.; Jacobsen, E. N. *J. Am. Chem. Soc.* **2004**, *126*, 1360. (e) Lu, X.-B.; Shi, L.; Wang, Y.-M.; Zhang, R.; Zhang, Y.-J.; Peng, X.-J.; Zhang, Z.-C.; Li, B. *J. Am. Chem. Soc.* **2006**, *126*, 1664. (f) Belser, T.; Jacobsen, E. N. *Adv. Synth. Catal.* **2008**, *350*, 967. (g) Kim, Y.-S.; Guo, X.-F.; Kim, G.-J. *Chem. Commun.* **2009**, 4296. (h) Zhu, X.; Venkatasubbaiah, K.; Weck, M.; Jones, C. W. *J. Mol. Catal. A: Chem.* **2010**, *329*, 1.

(14) Bailey, C. L.; Drago, R. S. *Coord. Chem. Rev.* **1987**, *79*, 321.

(15) Benisvy, L.; Bill, E.; Blake, A. J.; Collison, D.; Davies, E. S.; Garner, C. D.; Guindy, C. I.; McInnes, E. J. L.; McArdle, G.; McMaster, J.; Wilson, C.; Wolowska, J. *Dalton Trans.* **2004**, 3647.

(16) (a) Peng, P.-H.; Cheng, H.-Y.; Lin, C. C.; Peng, S. M. *Inorg. Chim. Acta* **1990**, *169*, 119. (b) Poddel'sky, A. I.; Cherkasov, V. K.; Fukin, G. K.; Bubnov, M. P.; Abakumova, L. G.; Abakumov, G. A. *Inorg. Chim. Acta* **2004**, *357*, 3632.

(17) Octahedral cobalt(II) complexes involving two semiquinonate ligands are often found to be in thermal equilibrium with their cobalt(III) valence tautomer involving a single semiquinonate and one catecholate ligand. Both valence states are very close in energy, see: (a) Kessel, S. L.; Emberson, R. M.; Debrunner, P. G.; Hendrickson, D. N. *Inorg. Chem.* **1980**, *19*, 1170. (b) Adams, D. M.; Die, A.; Rheingold, A. L.; Hendrickson, D. N. *J. Am. Chem. Soc.* **1993**, *115*, 8221. (c) Adams, D. M.; Noodleman, L.; Hendrickson, D. N. *Inorg. Chem.* **1997**, *36*, 3966. (d) Cador, O.; Chabre, F.; Dei, A.; Snagregorio, C.; Van Slageren, J.; Vaz, M. G. F. *Inorg. Chem.* **2003**, *42*, 6432. (e) Sato, O.; Cui, A.; Matsuda, R.; Tao, J.; Hayami, S. *Acc. Chem. Res.* **2007**, *40*, 361. (f) Dei, A.; Feis, A.; Poneti, G.; Sorace, L. *Inorg. Chim. Acta* **2008**, *361*, 3842. (g) Dapporto, P.; Die, A.; Poneti, G.; Sorace, L. *Chem.*−*Eur. J* **2008**, *14*, 10915. (h) Yoshida, Y.; Tanaka, H.; Saito, G.; Ouahab, L.; Yoshida, H.; Sato, N. *Inorg. Chem.* **2009**, *48*, 9989. (i) Evangelio, E.; Bonnet, M.-L.; Cabanas, M.; Nakano, M.; Sutter, J.-P.; Dei, A.; Robert, V.; Ruiz-Molina, D. *Chem.*−*Eur. J.* **2010**, *16*, 6666.

(18) (a) Herebian, D.; Ghosh, P.; Chun, H.; Bothe, E.; Weyhermüller, T.; Wieghardt, K. *Eur. J. Inorg. Chem.* **2002**, 1957. (b) Bill, E.; Both, E.; Chaudhuri, P.; Chlopek, C.; Herebian, D.; Kokatam, S.; Ray, K.; Weyhermüller, T.; Neese, F.; Wieghardt, K. *Chem. —Eur. J.* **2005**, *11*, 204.
(19) (a) Smith, A. L.; Clapp, L. A.; Hardcastle, K. I.; Soper, J. D. *Polyhedron* **2010**, *29*, 164. (b) Smith, A. L.; Hardcastle, K. I.; Soper, J. D. *J. Am. Chem. Soc.* **2010**, *132*, 14358. (c) Dzik, W. I.; van der Vlugt, J. I.; Reek, J. N. H.; de Bruin, B. *Angew. Chem., Int. Ed.* **2011**, *50*, 3356.
(20) (a) Ray, K.; Begum, A.; Weyhermüller, T.; Piligkos, S.; van Slageren, J.; Neese, F.; Wieghardt, K. *J. Am. Chem. Soc.* **2005**, *127*, 4403. (b) Ray, K.; Petrenko, T.; Wieghardt, K.; Neese, F. *Dalton Trans.* **2007**, 1552. (c) Sproules, S.; Kapre, R. R.; Roy, N.; Weyhermüller, T.; Wieghardt, K. *Inorg. Chim. Acta* **2010**, *363*, 2702.
(21) Kemper, S.; Hrobarik, P.; Kaupp, M.; Schlörer, N. E. *J. Am. Chem. Soc.* **2009**, *131*, 4172.
(22) *TEXSAN, Crystal Structure Analysis Package*; Molecular Structure, Corp.: The Woodlands, TX, 1992.
(23) Dolomanov, O. V.; Bourhis, L. J.; Gildea, R. J.; Howard, J. A. K.; Puschmann, H. *J. Appl. Crystallogr.* **2009**, *42*, 339.
(24) Kahn, O. *Molecular Magnetism*; VCH Publishers: New York, 1993.
(25) Neese, F. *ORCA—an ab initio, Density Functional and Semiempirical Program Package, 2.8.0*; Universität Bonn: Bonn, Germany, 2010.
(26) Neese, F. *J. Biol. Inorg. Chem.* **2006**, *11*, 702.
(27) Perdew, J. P. *Phys. Rev. B* **1986**, *33*, 8822.
(28) Perdew, J. P. *Phys. Rev. B* **1986**, *34*, 7406.
(29) Becke, A. D. *Phys. Rev. A* **1988**, *38*, 3098.
(30) Schäfer, A.; Huber, C.; Ahlrichs, R. J. *Chem. Phys.* **1994**, *100*, 5829.
(31) Neese, F. *J. Comput. Chem.* **2003**, *24*, 1740.
(32) Weigend, A. *Phys. Chem. Chem. Phys.* **2006**, *8*, 1057.
(33) Klamt, A.; Schürmann, G. *J. Chem. Soc., Perkin Trans. 2* **1993**, 793.
(34) Becke, A. D. *J. Chem. Phys.* **1993**, *98*, 5648.
(35) Lee, C.; Yang, W.; Parr, R. G. *Phys. Rev. B* **1988**, *37*, 785.
(36) Casida, M. E. In *Recent Advances in Density Functional Methods*; Chong, D. P., Ed.; World Scientific: Singapore, 1995.
(37) Stratmann, R. E.; Scuseria, G. E.; Frisch, M. J. *J. Chem. Phys.* **1998**, *109*, 8218.
(38) Bauernschmitt, R.; Ahlrichs, R. *Chem. Phys. Lett.* **1996**, 454.
(39) Hirata, S.; Head-Gordon, M. *Chem. Phys. Lett.* **1999**, *314*, 291.
(40) Hirata, S.; Head-Gordon, M. *Chem. Phys. Lett.* **1999**, *302*, 375.
(41) Neese, F.; Olbrich, G. *Chem. Phys. Lett.* **2002**, 170.
(42) Neese, F. *Inorg. Chim. Acta* **2002**, *337C*, 181.
(43) Barone, V. *Recent Advances in Density Functional Methods, Part 1*, Chong, D. P., Ed.; World Scientific: Singapore, 1996.
(44) Zhang, Y.-L.; Ruan, W.-J.; Zhao, X.-J.; Wang, H.-G.; Zhu, Z.-A. *Polyhedron* **2003**, *22*, 1535.
(45) Leung, W.-H.; Chan, E. Y. Y.; Chow, E. K. F.; Williams, I. D.; Peng, S.-M. *J. Chem. Soc., Dalton Trans.* **1996**, 1229.
(46) Avdeef, A.; Shaefer, W. P. *J. Am. Chem. Soc.* **1976**, *98*, 5153.
(47) Schenk, K. J.; Meghdadi, S.; Amirnasr, M.; Habibi, M. H.; Amiri, A.; Salehi, M.; Kashi, A. *Polyhedron* **2007**, *26*, 5448.
(48) Nishinaga, A.; Tajima, K.; Speiser, B.; Eichhorn, E/; Rieker, A.; Ohya-Nishiguchi, H.; Ishizu, K. *Chem. Lett.* **1991**, 1403.
(49) Oxidation of **1** and **2** by O_2 is initiated by the binding of one *N*-methylimidazole ligand to the apical position of the complex. An octahedral Co(III)−$O_2^{\bullet-}$ adduct is then formed (Gall, R. S.; Rogers, J. F.; Schaefer, W. P.; Christoph, G. G. *J. Am. Chem. Soc.* **1976**, *98*, 5135) and slowly converted in $[\mathbf{1}\text{-}\mathbf{im_2}]^+$ or $[\mathbf{2}\text{-}\mathbf{im_2}]^+$. The superoxo/ *N*-methylimidazole adducts of **1** and **2** are paramagnetic and show similar EPR spectra (Supporting Information). The superoxo adducts of **1** and **2** exhibit different rates for conversion into $[\mathbf{1}\text{-}\mathbf{im_2}]^+$ or $[\mathbf{2}\text{-}\mathbf{im_2}]^+$. After 1 h >95% of adduct is converted in the case of **1**, whereas only 50% is converted in the case of **2**.
(50) Selected metrical parameters for $[\mathbf{1}\text{-}\mathbf{im_2}](\mathbf{SbF_6})\cdot\mathbf{1.63}$ and $[\mathbf{1}\text{-}\mathbf{im_2}](\mathbf{Cl})\cdot\mathbf{4H_2O}$ are given in the Supporting Information.
(51) Marzilli, L. G.; Summers, M. F.; Bresciani-Pahor, N.; Zangrando, E.; Charland, J.-P.; Randaccio, L. *J. Am. Chem. Soc.* **1985**, *107*, 6880.
(52) Calligaris, M.; Minichelli, D.; Nardin, G.; Randaccio, L. *J. Chem. Soc. A* **1970**, 2411.
(53) Cohen, C. T.; Thomas, C. M.; Peretti, K. L.; Lobkovsky, E. B.; Coates, G. W. *Dalton Trans.* **2006**, 237.
(54) We performed calculations by replacing the water molecule by an acetate ligand in order to check the effect of the ligand charge on the electronic structure of $[\mathbf{1}\text{-}\mathbf{H_2O}]^+$ and $[\mathbf{2}\text{-}\mathbf{H_2O}]^+$. Both SOMOs are mainly metal centered (>75%), showing that these complexes are best described as paramagnetic high-spin cobalt(III) species (see ref 21). The Co(III) oxidation state is therefore accessible in the context of a charge compensation mechanism. The nature and especially the charge of the axial donor thus play a crucial role in stabilization of the Co(III)−L vs Co(II)−$L^{\bullet}$ valence isomer.
(55) Rotthaus, O.; Jarjayes, O.; Del Valle, C. P.; Philouze, C.; Thomas, F. *Chem. Commun.* **2007**, 4462.
(56) Pilbrow, J. R. *J. Magn. Reson.* **1978**, *31*, 479.
(57) (a) Charpin, P.; Nierlich, M.; Vigner, D.; Lance, M.; Thuéry, P.; Zarembowitch, J.; Yvoire, F. *J. Crystallogr. Spectrosc. Res.* **1988**, *18*, 71. (b) Thuéry, P.; Zarembowitch, J.; Michalowicz, A.; Kahn, O. *Inorg. Chem.* **1987**, *26*, 851. (c) Goodwin, H. A. *Top. Curr. Chem.* **2004**, *234*, 23.
(58) Earnshaw, A.; Hewlett, P. C.; King, E. A.; Larkworthy, L. F. *J. Chem. Soc. A* **1968**, 241.
(59) Kennedy, B. J.; Fallon, G. D.; Gatehouse, B. M. K. C.; Murray, K. S. *Inorg. Chem.* **1984**, *23*, 580.
(60) Das, U. K.; Bobak, J.; Fowler, C.; Hann, S. E.; Petten, C. F.; Dawe, L. N.; Decken, A.; Kerton, F. M.; Kozak, C. M. *Dalton Trans.* **2010**, *39*, 5462.
(61) (a) Furutachi, H.; Fujinami, S.; Suzuki, M.; Okawa, H. *J. Chem. Soc., Dalton Trans.* **2000**, 2761. (b) Costes, J. P.; Dahan, F.; Garcia-Tojal, J. *Chem.—Eur. J.* **2002**, *8*, 5430. (c) Kita, S.; Furutachi, H.; Okawa, H. *Inorg. Chem.* **1999**, *38*, 4038. (d) Makhankova, V. G.; Vassilyeva, O. Y.; Kokozay, V. N.; Skelton, B. W.; Reedijk, J.; Van Albada, G. A.; Sorace, L.; Gatteschi, D. *New J. Chem.* **2001**, *25*, 685.
(62) (a) Borta, A.; Gillon, B.; Gukasov, A.; Cousson, A.; Luneau, D.; Jeanneau, E.; Ciumacov, I.; Sakiyama, H.; Tone, K.; Mikuriya, M. *Phys. Rev. B* **2011**, 83. (b) Blake, A. B.; Sinn, E.; Yavari, A.; Moubaraki, B.; Murray, K. S. *Inorg. Chim. Acta* **1995**, *229*, 281. (c) Kahn, O.; Tola, P.; Coudanne, H. *Chem. Phys.* **1979**, *42*, 355. (d) Dojer, B.; Pevec, A.; Jagodic, M.; Kristl, M.; Drofenik, M. *Inorg. Chim. Acta* **2012**, *383*, 98. (e) Schmidt, R. D.; Shultz, D. A.; Martin, J. D. *Inorg. Chem.* **2010**, *49*, 3162. (f) Titis, J.; Boca, R. *Inorg. Chem.* **2011**, *50*, 11838. (g) Min, K. S.; DiPasquale, A. G.; Golen, J. A.; Rheingold, A. L.; Miller, J. S. *J. Am. Chem. Soc.* **2007**, *129*, 2360.
(63) (a) Boudreaux, E. A.; Mulay, L. N. *Theory and Application of Molecular Paramagnetism*; Wiley Interscience: New York, 1976. (b) Carlin, R. L. *Magneto-chemistry*; Springer: Berlin, 1986.
(64) (a) Zats, G. M.; Arora, H.; Lavi, R.; Yufit, D.; Benisvy, L. *Dalton Trans.* **2011**, *40*, 10889. (b) Shimazaki, Y.; Kabe, R.; Huth, S.; Tani, F.; Naruta, Y.; Yamauchi, O. *Inorg. Chem.* **2007**, *46*, 6083. (c) Müller, J.; Kikuchi, A.; Bill, E.; Weyhermüller, T.; Hildebrandt, P.; Ould-Moussa, L.; Wieghardt, K. *Inorg. Chim. Acta* **2000**, *297*, 265. (d) Sokolowski, A.; Adam, B; Weyhermüller, T.; Kikuchi, A.; Hilden-brand, K.; Schnepf, R.; Hildebrandt, P.; Bill, E.; Wieghardt, K. *Inorg. Chem.* **1997**, *36*, 3702. (e) Kimura, S.; Bill, E.; Bothe, E.; Weyhermüller, T.; Wieghardt, K. *J. Am. Chem. Soc.* **2001**, *123*, 6025.
(65) (a) Itoh, S.; Taki, M.; Takayama, S.; Nagatomo, S.; Kitagawa, T.; Sakurada, N.; Arakawa, R.; Fukuzumi, S. *Angew. Chem., Int. Ed.* **1999**, *38*, 2774. (b) Itoh, S.; Taki, M.; Kumei, H.; Takayama, S.; Nagatomo, S.; Kitagawa, T.; Sakurada, N.; Arakawa, R.; Fukuzumi, S. *Inorg. Chem.* **2000**, *39*, 3708. (c) Shimazaki, Y.; Huth, S.; Hirota, S.; Yamauchi, O. *Bull. Chem. Soc. Jpn.* **2000**, *73*, 1187. (d) Shimazaki, Y.; Huth, S.; Hirota, S.; Yamauchi, O. *Inorg. Chim. Acta* **2002**, *331*, 168. (e) Thomas, F.; Gellon, G.; Gautier-Luneau, I.; Saint-Aman, E.; Pierre, J.-L. *Angew. Chem., Int. Ed.* **2002**, *41*, 3047. (f) Shimazaki, Y.; Huth, S.; Hirota, S.; Yamauchi, O. *Inorg. Chim. Acta* **2002**, *331*, 168. (g) Philibert, A.; Thomas, F.; Philouze, C.; Hamman, S.; Saint-Aman, E.; Pierre, J.-L.

Chem.—Eur. J **2003**, *9*, 3803. (h) Michel, F.; Thomas, F.; Hamman, S.; Saint-Aman, E.; Bucher, C.; Pierre, J.-L. *Chem.—Eur. J.* **2004**, *10*, 4115. (i) Taki, M.; Hattori, H.; Osako, T.; Nagatomo, S.; Shiro, M.; Kitagawa, T.; Itoh, S. *Inorg. Chim. Acta* **2004**, *357*, 3369. (j) Michel, F.; Torelli, S.; Thomas, F.; Duboc, C.; Philouze, C.; Belle, C.; Hamman, S.; Saint-Aman, E.; Pierre, J.-L. *Angew. Chem., Int. Ed.* **2005**, *44*, 438. (k) Michel, F.; Thomas, F.; Hamman, S.; Philouze, C.; Saint-Aman, E.; Pierre, J.-L. *Eur. J. Inorg. Chem.* **2006**, 3684. (l) John, A.; Shaikh, M. M.; Ghosh, P. *Dalton Trans.* **2008**, 2815. (m) Michel, F.; Hamman, S.; Philouze, C.; Pérez Del Valle, C.; Saint-Aman, E.; Thomas, F. *Dalton Trans.* **2009**, 832.

(66) We investigated the electronic structure of $[\mathbf{1}]^{2+}$ by considering a pentacoordinated cobalt ion with one coordinated water molecule in a geometry directly derived from $[\mathbf{1}\text{-}\mathbf{H_2O}]^{+}$. A bis(phenoxyl) radical character was obtained for the dication, whose ground spin state is paramagnetic ($S = 3/2$).

(67) Kurahashi, T.; Fujii, H. *J. Am. Chem. Soc.* **2011**, *133*, 8307.